Analysis of Urban Two-Tier Heterogeneous Mobile Networks with Small Cell Partitioning

Martin Taranetz, *Member, IEEE,* Robert W. Heath Jr., *Fellow, IEEE,* and Markus Rupp, *Fellow, IEEE*

***Abstract*—In this work we investigate the performance of typical indoor users in urban two-tier heterogeneous mobile networks with indoor-deployed small cell base stations (BSs) and outdoor BSs. The urban topology is modeled by a Boolean scheme of blockages, which is tied together with the deployment of outdoor- and indoor BSs as well as the signal propagation characteristics. Each building is assumed to be served by an indoor small cell BS with a certain probability, which is denoted as occupation probability. Indoor and outdoor environments are partitioned by walls with a certain penetration loss. We separately account for outdoor BSs in line of sight (LOS) and non-line of sight (NLOS), as well as small cell BSs in neighboring and non-neighboring buildings. We derive expressions for the signal to interference ratio (SIR)-coverage probability and the average spectral efficiency of a typical indoor user. Numerical evaluations are performed with 3GPP compliant macro- and pico BS scenarios. Our results exhibit that the indoor area coverage, which is a function of the building density and size, significantly affects the impact of the target building's wall penetration loss. The analysis is simplified by various assumptions, which are verified by extensive Monte Carlo simulations.**

***Index Terms*—Small Cells; Heterogeneous Mobile Network; Urban Topology; Building Density; Boolean Model; Stochastic Geometry; Virtual Building Approximation;**

I. Introduction

It is estimated that the majority of today's mobile traffic originates and is consumed indoors [1]. Providing broadband radio access inside buildings by outdoor base stations (BSs) constitutes a significant challenge, as signals incur severe attenuation due to the wall penetration loss. This has given rise to the deployment of indoor small cell BSs, leading to *denser* and *more heterogeneous* mobile networks.

The case of dense small cell networks by means of stochastic geometry was first investigated in [2][3]. The authors reveal the invariance of the coverage probability and the spectral efficiency on the spatial density of the BSs as well as the number of tiers. A common assumption of these studies is the standard single-slope path loss model. More recent investigations in [4][5][6] show that this assumption may lead to fundamentally erroneous conclusions. It is commonly agreed that the discrepancies mainly arise from neglecting the distinct propagation conditions of line of sight (LOS) and non-line of sight (NLOS) signals. In an urban environment, LOS transmissions will occur when the distance between BS and user is small, while for larger distances, a transition from LOS to NLOS will appear with a higher likelihood. Studies incorporating both LOS and NLOS propagation conditions have recently been carried out in both the millimeter wave (mmWave) domain [7][8][9] as well as the below-6 GHz domain [4][6][10]. In this paper, we focus on urban heterogeneous networks operating below 6 GHz. Those mainly differ from mmWave networks by the fact that they are strongly interference limited.

While the presence of blockages is usually abstracted to some distance-dependent LOS probability function (see, e.g., [4][5][6][10][11], and also technical reports of the 3rd Generation Partnership Project (3GPP) [12][13]), modeling the *attenuation due to blockages* commonly lacks such a distance dependency or is omitted entirely [4][5][6][10]. A frequently used approach for describing the effects of large-scale blockages is the application of log-normally distributed random variables (RVs) [7]. In [14], it was argued that these RVs act as a random displacement of the original BS locations. Although the log-normal model exhibits a good agreement with measurement results, it requires an empirical calibration step. This not only limits its validity to a specific environment but also obscures the characteristics of the investigated topology, such as building density and size. Furthermore, recent studies within the 3GPP as well as in [15][16] indicate the impact of the blockages as a function of the distance.

Finally, scenarios consisting of *indoor- and outdoor environments* have not received much attention in analytical studies, due to the imposed inhomogeneities on the signal propagation. Moreover, measurement results in [17–19] indicate that LOS and NLOS signals experience significantly different wall penetration characteristics. While exhibiting a dependency on the angle of incidence in the LOS case, the wall loss yields a rather low value under NLOS conditions. Intuitively, this is caused by the fact that multi-path components approach the building more frontally after multiple reflections. Note that in the case of building penetration, the notions of *LOS* and *NLOS* refer to the signal propagation *outside* the target building.

Manuscript received November 6, 2015; revised March 22 2016; accepted July 21, 2016. Date of publication **tbd**; Date of current version August 2, 2016. This work has been funded by the Christian Doppler Laboratory for Dependable Wireless Connectivity for the Society in Motion. It is further based upon work supported in part by the National Science Foundation under Grant No. NSF-CCF-1319556. The financial support by the Austrian Federal Ministry of Science, Research and Economy is gratefully acknowledged. This work has been co-financed by A1 Telekom Austria AG and the INWITE project. The associate editor coordinating the review of this manuscript and approving it for publication was Prof. Stefano Buzzi. Parts of this paper appeared at the 11th International Symposium on Wireless Communication Systems (ISWCS'14), Barcelona, Spain, Aug. 26-29, 2014.

M. Taranetz and M. Rupp are with the Institute of Telecommunications, Technische Universität Wien, Vienna, Austria (e-mail: {mtaranet,mrupp}@nt.tuwien.ac.at).

R. W. Heath Jr. is with the Wireless Networking and Communications Group, University of Texas at Austin, Austin, TX, USA (e-mail: rheath@utexas.edu).

Digital Object Identifier **tbd**

A. Our Contributions

The main contribution of this paper is a stochastic geometry framework for analyzing signal to interference ratio (SIR)-coverage and spectral efficiency in an urban two-tier heterogeneous mobile network. Our focus is on the performance of a typical *indoor* user, as it has received much less attention in literature. The network comprises outdoor BSs in LOS and NLOS, as well as opportunistically deployed indoor small cell BSs. Indoor and outdoor environments are partitioned by a certain wall penetration loss, which is assumed to be different for LOS and NLOS transmissions.

The major challenge in establishing such model is to maintain a sufficient analytical tractability while reflecting key features of the real world environment with a small set of parameters. We employ a Boolean scheme of blockages and tie it together with the deployment of outdoor and indoor BS as well as the abstraction of the signal propagation. In this way, we establish an integrated framework, where each change of the urban topology directly affects the BS topology as well as the signal propagation characteristics. Since neither actual building footprints nor BS locations are required, which often constitute sensible and confidential information, our framework offers a transparent interface between network operators and industrial as well as academic research organizations.

We assume that each building is served by an indoor small cell with a certain probability, which we denote as *occupation probability*. When the user is located in a small cell-occupied building, it is considered to associate with the corresponding small cell BS. Otherwise, it will attach to an outdoor BS. We derive the probabilities to associate with the *strongest* outdoor BS in LOS or NLOS as well as the corresponding distance distributions. Moreover, we provide convenient expressions for the coverage probability in each situation.

We carry out numerical evaluations based on two 3GPP compliant setups. In the first setup, the outdoor BSs are represented by sparsely distributed macro BSs with a high transmit power, while in the second setup, they are constituted by densely deployed pico BSs with a low transmit power. Existing work often measures the spectral efficiency over the BS density. In this paper, we evaluate the performance over the indoor area coverage, which is a function of the building density and size. We show that the indoor area coverage alters the impact of the taget building's wall penetration loss. Throughout the paper, we make various assumptions to simplify the analysis. The validity of our model is gauged by extensive Monte Carlo simulations.

In this work, we focus on downlink transmissions. The major weakness of our model is the negligence of reflections, thus ignoring effects of gracing incidence and wave guidance, as reported, e.g., in [20]. At best, these effects are incorporated in the path loss exponent. Their explicit treatment provides an interesting topic for future work. For simplicity, we investigate buildings of circular shape. An extension to arbitrarily shaped building is carried out by means of the Minkowski sum [21] and beyond the scope of this paper. It considerably complicates the analysis while not improving the insights that can be drawn from it. We omit the inclusion of the building height. An extension is straightforwardly carried out along the lines of [15, Sec. III.B]. For the tractability of the analysis, we assume the LOS probabilities and building blockages between different links to be independent. In other words, we ignore potential correlations of buildings between links. According to [15], this only causes a minor loss of accuracy. A framework for investigating the performance of a typical *outdoor* user is rather extensive, and therefore exceeds the scope of this contribution.

B. Prior and Related Work

Compared to our prior work in [22], this paper provides a generalized mathematical framework that accounts for macro BSs in LOS and NLOS as well as the corresponding, generally distinct, wall penetration losses. In [22], we only considered interference from small cell BSs in neighboring buildings, which experience LOS conditions. In this paper, we also incorporate the interference from small cell BSs in non-neighboring buildings, experiencing NLOS conditions. It further includes the detailed mathematical derivations that are omitted in [22] due to space limitations. In [22], it was concluded that building blockage may have a beneficial impact on the performance as it provides a safeguard against interferers. In this contribution, we deepen our understanding on the impact of the urban environment by including LOS BS for which the blockage protection does not apply. The closest related works to the contribution in this paper are [4][5][6][15].

The authors of [4] consider a propagation model as provided by 3GPP in [12]. It is intended for heterogeneous networks at a carrier frequency of $2\,\mathrm{GHz}$ and formulates as

$$\ell(d) = \begin{cases} \frac{1}{c_\mathrm{L}} d^{-\alpha_L} & , v(d) \\ \frac{1}{c_\mathrm{N}} d^{-\alpha_N} & , 1 - v(d) \end{cases}, \tag{1}$$

where c_L and c_N are constants of the path loss law under LOS and NLOS conditions, α_L and α_N denote the corresponding path loss exponents and $v(d)$ refers to the probability of experiencing LOS propagation conditions at distance d. The authors derive a stochastic geometry framework for a *single tier network* and approximate the 3GPP LOS function from [12, Table A.2.1.1.2-3] by $v(d) = \exp(-(d/L)^2)$, where L is a tunable parameter. They observe a non-constant behavior of the spectral efficiency over the BS density, which is mainly caused by the split path loss law in (1).

Similar conclusions are drawn in [5], where the authors propose a multi-slope path loss model, which exhibits a sharp separation of the propagation characteristics at a certain distance. The approach is claimed to be very close to many scenarios in the WINNER II path loss model [12][23], and is well supported by measurements, e.g., [24].

In comparison to [5], the work in [6] provides a multi-slope path loss function, where each slope features probabilistic LOS and NLOS transmissions. Hence, it effectively combines the approaches in [4] and [5], yielding the most general path loss abstraction. Despite offering a high degree of freedom, the authors demonstrate the application of their model only with a single slope path loss model similar to (1). They investigate a simple linear LOS function $v(d)$, and show that it achieves

a good approximation of a more complicated function from 3GPP [12].

The authors in [15] establish an urban environment by means of a random object process (ROP), in particular a Boolean scheme, which is later explained in Section II-A. This technique neglects correlations among blockages, which is shown to have only a minor impact on its accuracy. The authors investigate a scenario with impenetrable blockages and introduce the concept of a *LOS ball*, which has found wide acceptance for the study of mmWave communication [9]. They are also the first to derive expressions for the *attenuation due to blockages* in ROP-based scenarios. It is observed that, on average, the blockages impose an exponential decay $\exp(-\beta\, d + p)$ on the received signal power, which depends on the link length d. The parameters β and p are conveniently derived from the properties of the ROP.

In comparison to our contribution, all works presented above focus on single-tier networks. Furthermore, the BS are considered to be outdoors, i.e., the partitioning due to wall penetration is omitted. Finally, except [15], they do not draw a connection between the LOS probability, the signal propagation model and the characteristics of the urban environment, such as building size and density.

C. Paper Organization

This paper is organized as follows. The system model is introduced in Section II. Section III presents the performance analysis. A numerical evaluation with respect to 3GPP compliant scenarios is carried out in Section IV. Section V concludes the paper.

II. System Model

In this section, we introduce the system model to evaluate the downlink performance of a typical indoor user in an urban two-tier mobile network. It is an extension of the model in [22] and incorporates the separation between macro BS in LOS and NLOS, as well as interference contribution from small cell BSs in non-neighboring buildings.

A. Topology Model for Urban Environments

Consider an urban environment with buildings that are modeled by a random object process [21]. We employ a Boolean scheme of circles on the $\mathbb{R}^2$ plane, as shown in Fig. 1. It satisfies the property that the centers of the circles form a Poisson point processes (PPP) Φ_{B} of intensity λ_{B} [21]. For simplicity, it is assumed that all circles have a fixed radius R_{I}. A point is denoted as *indoors*, if it is covered by building, and *outdoors* otherwise. The indoor and outdoor environment are partitioned by wall penetration loss, which is generally distinct in the LOS- and the NLOS case, respectively [17–19].

Define the *indoor coverage ratio* as the fraction of the total area on $\mathbb{R}^2$ that is covered by buildings. According to [15, Corollary 1.2], for the specified Boolean scheme, it is calculated as

$$p_{\mathrm{I}} = 1 - e^{-\lambda_{\mathrm{B}} R_{\mathrm{I}}^2 \pi}. \tag{2}$$

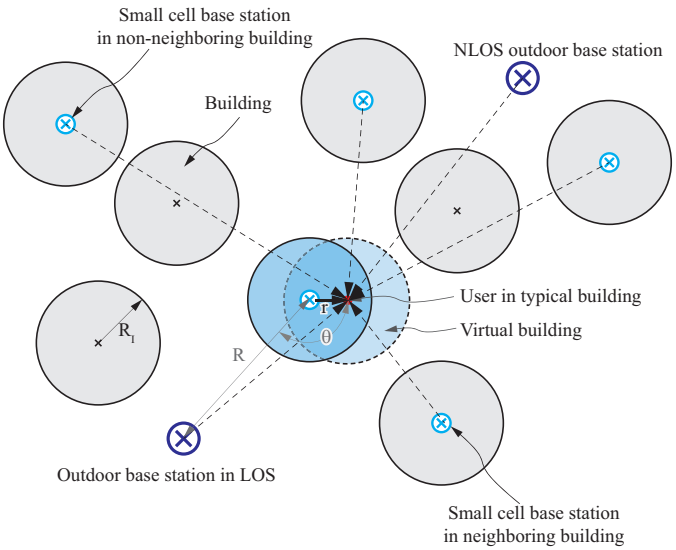

Fig. 1: Snapshot of an urban environment as obtained by a Boolean scheme with circles of fixed radius R_{I}. The figure depicts an indoor user in a typical building, which is occupied by a small cell BS. The scenario encompasses LOS- and NLOS outdoor BSs as well as small cell BSs in neighboring and non-neighboring buildings. The dashed circle indicates a virtual building around the user, as presented in Section II-D.

The indoor coverage ratio has the remarkable feature that it can also be extracted from real-world data [7][25]. For example, the OpenStreetMap project provides open access to *shape files*, which, among other information, contain the building footprints. These files can be processed by a simple MATLAB script. For The University of Texas at Austin and Vienna's inner district ratios of $p_{\mathrm{I}} = 0.25$ and $p_{\mathrm{I}} = 0.5$ were measured. Related work in [25] evaluated the indoor coverage of various Turkish cities. The ratios ranged from $0.13 - 0.39$. The authors in [7] evaluated Manhattan and the city of Chicago, where values of 0.46 an 0.42 were found. In the following, the Boolean model is applied to model the urban environment which serves as a basis for the deployment of a two-tier heterogeneous mobile network.

B. Network Deployment

In this section, we explain the deployment of a two-tier mobile network in the introduced urban environment. The network comprises outdoor BSs and indoor-deployed small cell BSs, as shown in Fig. 1. The outdoor BSs are distributed according to a PPP Φ_{O} of intensity μ_{O}. Since we require these BSs to be located outdoors, the BS process can equivalently be established by *independently thinning* (see, e.g., [21]) an initial PPP of intensity $\mu'_{\mathrm{O}} = \mu_{\mathrm{O}}/(1 - p_{\mathrm{I}})$, with p_{I} from (2).

A building will be served by an indoor small cell BS with a certain probability η, which we denote as *occupation probability*. Consider the indoor small cell BSs to be located at the center points of the occupied buildings. Then, the spatial distribution of the indoor small cell BSs can be modeled by a PPP Φ_{S} of intensity $\eta\, \lambda_{\mathrm{B}}$, which follows from independently thinning the object center PPP Φ_{B}.

C. Signal propagation

In this section, we introduce models to describe the signal propagation. As illustrated in Fig. 1, the typical indoor user experiences various types of links.

1) Outdoor BS to Indoor User: We assume that a signal originating from an outdoor BS experiences small scale fading, log-distance dependent path loss, attenuation due to building blockage and wall penetration. The small scale fading is modeled by independent RVs $G_{\mathrm{L},i}$, $G_{\mathrm{N},i}$ and $G_{\mathrm{I},i}$, accounting for the fact that, in general, LOS-, NLOS- and indoor transmissions will exhibit distinct fading distributions. For signal propagation in the LOS- and the NLOS case, we formulate the following path loss laws:

$$\ell_{\mathrm{L}}(R) = \frac{1}{c_{\mathrm{L}}} R^{-\alpha_{\mathrm{L}}} L_{\mathrm{L}}, \tag{3}$$

$$\ell_{\mathrm{N}}(R) = \frac{1}{c_{\mathrm{N}}} R^{-\alpha_{\mathrm{N}}} B_{\mathrm{N}}(R) L_{\mathrm{N}}, \tag{4}$$

where c_{L} and c_{N} are the constants of the path loss law, L_{L} and L_{N} denote wall penetration losses for LOS and NLOS signals, and $B_{\mathrm{N}}(\cdot)$ refers to the attenuation due to blockage by buildings, respectively. In this work we employ the expected blockage attenuation as referred from [15, Theorem 6]. Then, $B_{\mathrm{N}}(R)$ in (4) is obtained as

$$B_{\mathrm{N}}(R) = e^{-\beta_{\mathrm{B}} R(1-L_{\mathrm{B}})}, \tag{5}$$

where L_{B} refers to the attenuation of a single blockage, also denoted as *building penetration loss*. Note that signal attenuation due to building blockage is fully quantified by an additional exponential path loss term in (4). Furthermore, (5) exclusively comprises parameters of the urban environment topology, in particular, building density, size and -penetration loss.

2) Small Cell BS to Indoor User: When user and small cell BS are situated in the same building, the signal experiences small scale fading and path loss according to

$$\ell_{\mathrm{I}}(r) = \frac{1}{c_{\mathrm{I}}} r^{-\alpha_{\mathrm{I}}}, \tag{6}$$

where c_{I} is the path loss constant. Since the small cell transmit power is generally low, in [22] small cell BSs are only taken into account as interferers, when they are situated in a *neighboring building*. Two buildings are defined as being neighbors, if the segment connecting their centers is not intersected by any other building. In this paper, we account for the interference from small cell BSs in both neighboring and non-neighboring buildings. The signals from small cell BSs in neighboring buildings are subject to small scale fading, log-distance dependent path loss under LOS conditions according to (3) and attenuation by a factor L_{W}, caused by the indoor-to-outdoor wall penetration. Small cell BSs in non-neighboring buildings are assumed to experience the same propagation conditions, except that the NLOS path loss from (4) is used instead of (3). Note that in general the parameters in (3) and (4) will be different for outdoor BS and indoor small cell BSs.

D. User Association

This contribution aims at characterizing the coverage and rate performance of a typical indoor user that is located at a certain distance away from the center of its building. Observing that the building centers form a PPP on $\mathbb{R}^2$, we can fix a *typical building* at the origin while the other buildings still constitute a PPP by virtue of Slivnyak's theorem [21]. In the following, we scrutinize a user within the typical building. Depending on whether or not a building is occupied by a small cell BS, separate association policies are defined.

[Policy SC]: Consider a typical building at the origin that is *occupied by a small cell BS*. For simplicity, it is assumed that a user associates to this BS throughout the entire building. Hence, we ignore the cases where the user might receive the strongest signal from an outdoor BS, and denote this assumption as *[Assoc-Asmp-1]*. This approximation yields a lower bound on the coverage probability. Along the lines of [26], *exclusion guard regions* are imposed on both outdoor- and small cell tier. They are designed to avoid the case where an interfering node is located within the typical building. For reasons of simplification, the exclusion region for outdoor BS is specified as a ball of radius R_{I} centered at the origin. It guarantees that no outdoor BS are located inside the typical building. For small cell BSs, the exclusion region is specified as a ball of radius $2\,R_{\mathrm{I}}$ so as to prevent two small cells from having overlapping association regions.

[Policy DM]: When the typical building is *not served* by a small cell BS, the user either attaches to the *dominant outdoor BS* or the strongest small cell BS in the immediate vicinity. We deem the *dominant-outdoor* association as being of greater relevance and omit the case of associating the user with a close-by small cell BS. This assumption is denoted as *[Assoc-Asmp-2]*. Similar to the approximation in *[Policy SC]*, it leads to a lower bound on the coverage probability. The indoor user will attach to the dominant outdoor BS, which could either be in LOS or NLOS, respectively. An outdoor BS is said to be in LOS, if the direct link between the user and the BS is not obstructed by a blockage. The same exclusion regions as defined in *[Policy SC]* are applied for outdoor- and small cell BSs.

Now consider a typical building at the origin and, without loss of generality, an indoor user at location $(r, 0)$ with $0 < r \leq R_{\mathrm{I}}$. Further, let the i-th outdoor BS be located at (R, θ), as illustrated in Fig. 1. Its distance to a user at $(r, 0)$ is determined as $d(r) = \sqrt{R^2 + r^2 - 2\,R\,r\,\cos(\theta)}$. Note that the exclusion regions as defined above are centered at the origin rather than at the user. Consequently, the interference field as observed by the user is *asymmetric* and renders analysis difficult in general. Since typically $R \gg r$, we can approximate $d(r)$ by $d(r) \approx R$. As shown in Fig. 1, this is equivalent to shifting all the BSs along with the exclusion regions by a vector $(r, 0)$, as if the typical building was centered at the user location [22]. We refer to this approximation as *[VBl-Approx]*.

Then, using the Boolean scheme as specified in Section II-A and *[VBl-Approx]*, the probability that the link between a user and an outdoor BS is obstructed by any other building is obtained as $v(R) = \exp(-\beta_{\mathrm{B}}(R - R_{\mathrm{I}}))$, with $\beta_{\mathrm{B}} = 2\,\lambda_{\mathrm{B}} R_{\mathrm{I}}$. This

term can be interpreted as the *LOS probability*. Intuitively, it becomes increasingly unlikely to experience a LOS connection with a distant BS. The negative exponential characteristic is also found in [8][15] and is remarkably consistent with the 3GPP standard [12][13]. In comparison to [4], it does not require an empirical calibration step, as it only comprises statistical parameters of the urban topology. If not stated otherwise, we will use $v(r)$ as introduced above. It should be noted that our analysis is general enough to allow for any $v(R)$.

According to [15], the shadowing of different links can be considered as uncorrelated with minor loss of accuracy. This allows to apply the thinning property of PPPs (see, e.g., [21]) on the outdoor BS process Φ_{M}, yielding two independent BS processes Φ_{L} and Φ_{N} for LOS and NLOS with intensities $\mu_{\mathrm{O}}\, v(R)$ and $\mu_{\mathrm{O}}\,(1 - v(R))$, respectively.

The following lemmas provide probability density functions (PDFs) for the distance between an indoor user and its associated outdoor BS, given that the BS is either in LOS or NLOS. The expressions extend results in [27] by conditioning on deploying a *virtual building* around the user, as illustrated in Fig. 1.

Lemma 1. *Consider a typical building without a small cell BS and an indoor user at distance r, $0 < r \leq R_{\mathrm{I}}$, away from its center, which is associated with the closest LOS outdoor BS. Then, applying the virtual building approximation, the associated users' distance to the serving BS is distributed as*

$$f_{\mathrm{L}}(r) = \begin{cases} \frac{B_{\mathrm{L}} \hat{f}_{\mathrm{L}}(r)}{A_{\mathrm{L}}} e^{-2\pi\mu_{\mathrm{O}} \int_{R_{\mathrm{I}}}^{\Psi_{\mathrm{L}}(r)} (1-v(t))t dt} & x \geq R_{\mathrm{I}} \\ 0 & \text{otherwise} \end{cases}, \tag{7}$$

where

$$B_{\mathrm{L}} = 1 - e^{-2\pi\mu_{\mathrm{O}} \int_{R_{\mathrm{I}}}^{\infty} v(t) t dt} \tag{8}$$

$$\hat{f}_{\mathrm{L}}(r) = \begin{cases} \frac{1}{B_{\mathrm{L}}} 2\pi\mu_{\mathrm{O}} x v(r) e^{-2\pi\mu_{\mathrm{O}} \int_{R_{\mathrm{I}}}^{r} v(t) t dt} & x \geq R_{\mathrm{I}} \\ 0 & \text{otherwise} \end{cases} \tag{9}$$

$$A_{\mathrm{L}} = B_{\mathrm{L}} \int_{R_{\mathrm{I}}}^{\infty} e^{-2\pi\mu_{\mathrm{O}} \int_{R_{\mathrm{I}}}^{\Psi_{\mathrm{L}}(x)} (1-v(t)) t dt} \hat{f}_{\mathrm{L}}(x) dx, \tag{10}$$

and $\Psi_{\mathrm{L}}(x) = \ell_{\mathrm{L}}^{-1}(\ell_{\mathrm{N}}(x))$.

The term B_{L} denotes the probability that the user receives at least one LOS BS and $\hat{f}_{\mathrm{L}}(x)$ is the corresponding conditional distance distribution function of the closest node. The quantity A_{L} captures the likelihood to be associated with the closest LOS BS.

Proof. The proof is provided in Appendix A. □

Intuitively, the term B_{L} in (8) represents the likelihood of a user having at least one outdoor BS in LOS. It increases with a larger base station density μ_{O} and a smaller building density and size, as incorporated in the term $v(r)$. It takes on the value zero, when the indoor coverage ratio $p_{\mathrm{I}} = 1$, and one, when $p_{\mathrm{I}} = 0$. Having at least one outdoor BS in LOS, the distance distribution $\hat{f}_{\mathrm{L}}(x)$ accounts for the distance-dependent thinning of the outdoor BS PPP, retaining only those BSs that are in LOS. Even if there is at least one outdoor BS in LOS, this does not imply that the user associates with it. In fact, this is only the case when the equivalent distance $\Psi_{\mathrm{L}}(x)$ to the LOS BS in terms of path loss is smaller than the distance to the nearest NLOS BS. The probability of this event is expressed by the term A_{L}. Finally, note that (7) is independent of the users location within the target building by virtue of the virtual building approximation.

Lemma 2. *Consider an indoor user at distance r, $0 < r \leq R_{\mathrm{I}}$ away from the center of a typical building without a small cell BS. Let the user be attached to the closest NLOS BS. Then, employing the virtual building approximation, the PDF of its distance to the serving BS is expressed as*

$$f_{\mathrm{N}}(r) = \begin{cases} \frac{B_{\mathrm{N}} \hat{f}_{\mathrm{N}}(r)}{A_{\mathrm{N}}} e^{-2\pi\mu_{\mathrm{O}} \int_{R_{\mathrm{I}}}^{\Psi_{\mathrm{N}}(r)} v(t)\, t\, dt} & x \geq R_{\mathrm{I}} \\ 0 & \text{otherwise} \end{cases}, \tag{11}$$

where

$$B_{\mathrm{N}} = 1 - e^{-2\pi\mu_{\mathrm{O}} \int_{R_{\mathrm{I}}}^{\infty} (1-v(t)) t dt} \tag{12}$$

$$\hat{f}_{\mathrm{N}}(r) = \begin{cases} \frac{1}{B_{\mathrm{N}}} 2\pi\mu_{\mathrm{O}} x (1 - v(r)) e^{-2\pi\mu_{\mathrm{O}} \int_{R_{\mathrm{I}}}^{r} (1-v(t))\, t\, dt} & x \geq R_{\mathrm{I}} \\ 0 & \text{otherwise} \end{cases} \tag{13}$$

$$A_{\mathrm{N}} = 1 - A_{\mathrm{L}}, \tag{14}$$

with A_{L} from (10) and $\Psi_{\mathrm{N}}(x) = \ell_{\mathrm{N}}^{-1}(\ell_{\mathrm{L}}(x))$.

The term B_{N} refers to the probability that the user receives at least one NLOS outdoor BS and $\hat{f}_{\mathrm{N}}$ is the according conditional PDF of the distance to the nearest node.

Proof. The proof is carried out along the lines of Appendix A. □

Applying (3) and (4) in Lemmas 1 and 2, $\Psi_{\mathrm{L}}(x)$ and $\Psi_{\mathrm{N}}(x)$ are calculated as

$$\Psi_{\mathrm{L}}(x) = \frac{\alpha_{\mathrm{N}}\, W\left(-\frac{1}{\alpha_{\mathrm{N}}}(-1 + L_{\mathrm{B}}) \left(\frac{c_{\mathrm{N}} L_{\mathrm{L}} x^{-\alpha_{\mathrm{L}}}}{c_{\mathrm{L}} L_{\mathrm{N}}}\right)^{-1/\alpha_{\mathrm{N}}} \beta_{\mathrm{B}}\right)}{(-1 + L_{\mathrm{B}})\beta_{\mathrm{B}}}, \tag{15}$$

$$\Psi_{\mathrm{N}}(x) = \left(\frac{c_{\mathrm{L}} e^{-(1-L_{\mathrm{B}}) x\, \beta_{\mathrm{B}}} L_{\mathrm{N}} x^{-\alpha_{\mathrm{N}}}}{c_{\mathrm{N}} L_{\mathrm{L}}}\right)^{-1/\alpha_{\mathrm{L}}}, \tag{16}$$

where $W(\cdot)$ refers to the Lambert W function. Intuitively, Ψ_{L} and Ψ_{N} refer to equivalent distances to the strongest LOS and NLOS BS with respect to the path loss. They are affected by the path loss exponents and exponents, the building penetration loss L_{B}, the wall penetration losses L_{L} and L_{N} as well as the parameter β_{B}, which encompasses building density and size. Remarkably, the distance of the dominant NLOS BS exhibits a logarithmic growth with the distance of the strongest outdoor BS in LOS. Conversely, the distance of the dominant BS in LOS increases exponentially with the distance of the strongest NLOS BS.

Next, we investigate the average number of outdoor BSs in LOS. Let Q_0 denote the visible area around a building of radius R_{I} that is centered at the origin. The average number of BSs in LOS is obtained by multiplying the average size of the visible region $\mathbb{E}[Q_0]$ by the BS density μ_{O}. Along the

lines of [15, Theorem 7],

$$\mu_{\mathrm{O}}\,\mathbb{E}[Q_0] = \mu_{\mathrm{O}}\,2\pi\int_{R_{\mathrm{I}}}^{\infty}\frac{r^2}{2}\beta_{\mathrm{B}}e^{-\beta_{\mathrm{B}}\,(r-R_{\mathrm{I}})}dr = \mu_{\mathrm{O}}\,\frac{\pi(2+R_{\mathrm{I}}\beta_{\mathrm{B}}(2+R_{\mathrm{I}}\beta_{\mathrm{B}}))}{\beta_{\mathrm{B}}^2}. \tag{17}$$

We observe that, in order to maintain a certain average number of outdoor BS in LOS, the BS density μ_{O} has to scale roughly quadratically with the building density λ_{B}, which is contained in β_{B}. Hence, increasing the BS density proportionately with the building density, the average number of BSs in LOS will decrease.

III. Performance Analysis

In this section we derive analytical expressions for the SIR-coverage probability of an indoor user at position $(r,0)$, regarding both buildings with- and without small cell deployment. We assume the network to be interference limited, as is typically the case in urban areas [28]. Therefore, thermal noise is neglected in the analysis. We denote this assumption as *[Int-Asmp]*.

A. Signal-to-Interference Ratio (SIR)

In a first step, we formulate the SIRs γ_a of a user in a typical building that is either associated with a small cell BS ($a=\mathrm{S}$) or a macro BS in LOS- or NLOS ($a=\{\mathrm{L},\mathrm{N}\}$), respectively. Then, we derive expressions for the SIR-coverage probability, which is commonly defined as the probability that the SIR γ_a exceeds some threshold δ, i.e., $P_{\mathrm{c},a}(\delta)=\mathbb{P}[\gamma_a>\delta]$ (see, e.g., [2]).

Given an indoor user at distance r, $0<r\leq R_{\mathrm{I}}$ away from the center of a typical building with small cell BS, its SIR is obtained as

$$\gamma_{\mathrm{S}}(r)=\frac{P_{\mathrm{O}}G_{\mathrm{I},0}\ell_{\mathrm{I}}(r)}{\Sigma_{\mathrm{L}}+\Sigma_{\mathrm{N}}+\Sigma_{\mathrm{S}}+\Sigma_{\overline{\mathrm{S}}}}, \tag{18}$$

where

$$\Sigma_{\mathrm{L}}=\sum_{\substack{i:x_i\in\Phi_{\mathrm{L}}\\ \setminus\mathcal{B}(0,R_{\mathrm{I}})}}P_{\mathrm{O}}G_{\mathrm{L},i}\ell_{\mathrm{L}}(\|x_i\|), \tag{19}$$

$$\Sigma_{\mathrm{N}}=\sum_{\substack{j:x_j\in\Phi_{\mathrm{N}}\\ \setminus\mathcal{B}(0,R_{\mathrm{I}})}}P_{\mathrm{O}}G_{\mathrm{N},j}\ell_{\mathrm{N}}(\|x_j\|), \tag{20}$$

$$\Sigma_{\mathrm{S}}=\sum_{\substack{k:x_k\in\Phi_{\mathrm{S}}\\ \setminus\mathcal{B}(0,2R_{\mathrm{I}})}}S_kP_{\mathrm{S}}G_{\mathrm{I},k}L_{\mathrm{W}}\ell_{\mathrm{L}}(\|x_k\|), \tag{21}$$

$$\Sigma_{\overline{\mathrm{S}}}=\sum_{\substack{k:x_k\in\Phi_{\mathrm{S}}\\ \setminus\mathcal{B}(0,2R_{\mathrm{I}})}}\overline{S}_kP_{\mathrm{S}}G_{\mathrm{I},k}L_{\mathrm{W}}\ell_{\mathrm{N}}(\|x_k\|), \tag{22}$$

where Σ_{L} and Σ_{N} refer to the aggregate interference from the outdoor BS in LOS and NLOS, and Σ_{S} and $\Sigma_{\overline{\mathrm{S}}}$ are the cumulative interferences from small cell BSs in neighboring and non-neighboring buildings. The terms P_{O} and P_{S} denote the transmit power of outdoor BSs and small cell BSs, respectively. The RVs $S_k\in\{0,1\}$ and $\overline{S}_k\in\{0,1\}$ are indicators whether or not a small cell BS is located in a neighboring building of the typical user (see Section II-C). Along the lines of [15], S_k and $\overline{S}_k$ are Bernoulli distributed with parameters $\exp(-\beta_{\mathrm{B}}R_{\mathrm{I}}-p_{\mathrm{B}})$ and $1-\exp(-\beta_{\mathrm{B}}R_{\mathrm{I}}-p_{\mathrm{B}})$, respectively, where $p_{\mathrm{B}}=\lambda_{\mathrm{B}}R_{\mathrm{I}}^2\pi$. Intuitively, the larger the distance to the typical indoor user, the less likely a building will be a *neighboring* building. The term $\mathcal{B}(0,x)$ denotes a sphere of radius x that is located at the origin.

When the building is not occupied by a small cell BS, the user associates with the dominant macro BS at distance R_0, with $R_0>R_{\mathrm{I}}$. Depending on whether the serving BS is in LOS or NLOS, then either

$$\gamma_{\mathrm{L}}(r)=\frac{P_{\mathrm{O}}G_{\mathrm{L},0}\ell_{\mathrm{L}}(R_0)}{\Sigma'_{\mathrm{L}}+\Sigma'_{\mathrm{N}}+\Sigma_{\mathrm{S}}+\Sigma_{\overline{\mathrm{S}}}}, \tag{23}$$

or

$$\gamma_{\mathrm{N}}(r)=\frac{P_{\mathrm{O}}G_{0}\ell_{\mathrm{N}}(R_0)}{\Sigma''_{\mathrm{L}}+\Sigma''_{\mathrm{N}}+\Sigma_{\mathrm{S}}+\Sigma_{\overline{\mathrm{S}}}}, \tag{24}$$

where

$$\Sigma'_{\mathrm{L}}=\sum_{\substack{i:x_i\in\Phi_{\mathrm{L}}\\ \setminus\mathcal{B}(0,R_0)}}P_{\mathrm{O}}G_{\mathrm{L},i}\ell_{\mathrm{L}}(\|x_i\|), \tag{25}$$

$$\Sigma'_{\mathrm{N}}=\sum_{\substack{j:x_j\in\Phi_{\mathrm{N}}\\ \setminus\mathcal{B}(0,\Psi_{\mathrm{L}}(R_0))}}P_{\mathrm{O}}G_{\mathrm{N},j}\ell_{\mathrm{N}}(\|x_j\|), \tag{26}$$

$$\Sigma''_{\mathrm{L}}=\sum_{\substack{i:x_i\in\Phi_{\mathrm{L}}\\ \setminus\mathcal{B}(0,\Psi_{\mathrm{N}}(R_0))}}P_{\mathrm{O}}G_{\mathrm{L},i}\ell_{\mathrm{L}}(\|x_i\|), \tag{27}$$

$$\Sigma''_{\mathrm{N}}=\sum_{\substack{j:x_j\in\Phi_{\mathrm{N}}\\ \setminus\mathcal{B}(0,R_0)}}P_{\mathrm{O}}G_{\mathrm{N},j}\ell_{\mathrm{N}}(\|x_j\|). \tag{28}$$

By virtue of *[VBl-Approx]* (conf. Section II-D) both $\gamma_{\mathrm{L}}(\cdot)$ and $\gamma_{\mathrm{N}}(\cdot)$ are *independent* of the user's location within the building.

B. SIR Coverage

Next, we derive expressions for the SIR-coverage of an indoor user in a typical building. The following theorems extend [22, Theorems 1 and 2] with respect to LOS- and NLOS macro BSs and also account for small cell BSs in non-neighboring buildings. For simplicity, we assume Rayleigh fading along the indoor- and NLOS links, while the LOS transmissions are considered to experience Nakagami-m fading with $\Omega=1$ and $m=N_{\mathrm{L}}$. To further facilitate matters, we assume that $N_{\mathrm{L}}\in\mathbb{N}^+$ [27, 29].

Theorem III.1. *Consider an indoor user at distance r, $0<r\leq R_{\mathrm{I}}$ away from the center of a typical building with a small cell BS. Then, its SIR-coverage probability is calculated as*

$$P_{c,\mathrm{S}}(\delta|r)=\mathbb{P}\left[\gamma_{\mathrm{S}}(r)>\delta|r\right]=e^{-2\pi(\mu_{\mathrm{S}}(I_{\mathrm{S}}+I_{\overline{\mathrm{S}}})+\mu_{\mathrm{O}}(I_{\mathrm{L}}+I_{\mathrm{N}}))}, \tag{29}$$

with $\gamma_{\mathrm{S}}(\cdot)$ from (18) and

$$I_{\mathrm{L}}=\int_{R_{\mathrm{I}}}^{\infty}\left(1-\left(1+\frac{\delta\,\ell_{\mathrm{L}}(t)}{\frac{P_{\mathrm{S}}}{P_{\mathrm{O}}}\,\ell_{\mathrm{I}}(r)\,N_{\mathrm{L}}}\right)^{-N_{\mathrm{L}}}\right)t\,v(t)\,dt, \tag{30}$$

$$I_{\mathrm{N}}=\int_{R_{\mathrm{I}}}^{\infty}\left(1-\frac{\frac{P_{\mathrm{S}}}{P_{\mathrm{O}}}\ell_{\mathrm{I}}(r)}{\frac{P_{\mathrm{S}}}{P_{\mathrm{O}}}\ell_{\mathrm{I}}(r)+\delta\,\ell_{\mathrm{N}}(t)}\right)t\,(1-v(t))dt, \tag{31}$$

$$I_{\mathrm{S}}=\int_{2\,R_{\mathrm{I}}}^{\infty}\left(1-\left(1+\frac{\delta\,L_W\ell_{\mathrm{L}}(t)}{\ell_{\mathrm{I}}(r)\,N_{\mathrm{L}}}\right)^{-N_{\mathrm{L}}}\right)e^{-(\beta_{\mathrm{B}}t+p_{\mathrm{B}})}\,t\,dt, \tag{32}$$

$$I_{\overline{\mathrm{S}}} = \int_{2R_\mathrm{I}}^{\infty} \frac{\delta L_\mathrm{W} \ell_\mathrm{N}(t)}{\ell_\mathrm{I}(r) + \delta L_\mathrm{W} \ell_\mathrm{N}(t)} \left(1 - e^{-(\beta_\mathrm{B} t + p_\mathrm{B})}\right) t\, dt. \tag{33}$$

Proof. The proof is provided in Appendix B. □

Theorem III.2. *Consider a typical building without a small cell BS and an indoor user at distance r, $0 < r \le R_\mathrm{I}$ away from its center. Given that the user is associated with the closest LOS outdoor BS, its SIR-coverage probability is determined as*

$$P_{c,\mathrm{L}} = \mathbb{P}\left[\mathbb{E}_{R_0}[\gamma_\mathrm{L}(R_0) > \delta]\right] = \int_{R_\mathrm{I}}^{\infty} \left(\sum_{n=1}^{N_\mathrm{L}} (-1)^{n+1} \binom{N_\mathrm{L}}{n} e^{-2\pi(\mu_\mathrm{S}(I_\mathrm{S} + I_{\overline{\mathrm{S}}}) + \mu_\mathrm{O}(I_\mathrm{L} + I_\mathrm{N}))} \right) f_\mathrm{L}(R) dR \tag{34}$$

with $\gamma_\mathrm{L}(\cdot)$ from (23), $f_\mathrm{L}(\cdot)$ from (7) and

$$I_\mathrm{L} = \int_{R_0}^{\infty} \left(1 - \left(1 + \frac{n\, \nu_\mathrm{L}\, \delta\, \ell_\mathrm{L}(t)}{\ell_\mathrm{L}(R_0)\, N_\mathrm{L}}\right)^{-N_\mathrm{L}}\right) t\, v(t) dt, \tag{35}$$

$$I_\mathrm{N} = \int_{\Psi_\mathrm{L}(R)}^{\infty} \left(1 - \frac{\ell_\mathrm{L}(R)}{\ell_\mathrm{L}(R) + n\, \nu_\mathrm{L}\, \delta\, \ell_\mathrm{N}(t)}\right) t\, (1 - v(t)) dt, \tag{36}$$

$$I_\mathrm{S} = \int_{2\,R_\mathrm{I}}^{\infty} \left(1 - \left(1 + \frac{n\, \nu_\mathrm{L}\, \delta\, \frac{P_\mathrm{S}}{P_\mathrm{O}}\, L_W \ell_\mathrm{L}(t)}{\ell_\mathrm{L}(R_0)\, N_\mathrm{L}}\right)^{-N_\mathrm{L}}\right) e^{-(\beta_\mathrm{B} t + p_\mathrm{B})}\, t\, dt, \tag{37}$$

$$I_{\overline{\mathrm{S}}} = \int_{2R_\mathrm{I}}^{\infty} \frac{n\, \nu_\mathrm{L}\, \delta\, \frac{P_\mathrm{S}}{P_\mathrm{O}} L_\mathrm{W} \ell_\mathrm{N}(t)}{\ell_\mathrm{L}(R) + n\, \nu_\mathrm{L}\, \delta\, \frac{P_\mathrm{S}}{P_\mathrm{O}} L_\mathrm{W} \ell_\mathrm{N}(t)} \left(1 - e^{-(\beta_\mathrm{B} t + p_\mathrm{B})}\right) t\, dt, \tag{38}$$

with $\nu_\mathrm{L} = N_\mathrm{L}(N_\mathrm{L}!)^{-1/N_\mathrm{L}}$.

When the user is served by the closest NLOS outdoor BS, its SIR-coverage probability is calculated as

$$P_{\mathrm{c,N}}(\delta) = \mathbb{P}\left[\mathbb{E}_{R_0}[\gamma_\mathrm{N}(R_0) > \delta]\right] = \int_{R_\mathrm{I}}^{\infty} e^{-2\pi(\mu_\mathrm{S}(I_\mathrm{S} + I_{\overline{\mathrm{S}}}) + \mu_\mathrm{M}(I_\mathrm{L} + I_\mathrm{N}))} f_\mathrm{N}(R) dR \tag{39}$$

where $\gamma_\mathrm{N}(\cdot)$ and $f_\mathrm{N}(\cdot)$ are obtained from (11) and (24), and

$$I_\mathrm{L} = \int_{\Psi_\mathrm{N}(R_0)}^{\infty} \left(1 - \left(1 + \frac{\delta\, \ell_\mathrm{L}(t)}{\ell_\mathrm{N}(R_0)\, N_\mathrm{L}}\right)^{-N_\mathrm{L}}\right) t\, v(t) dt, \tag{40}$$

$$I_\mathrm{N} = \int_{R}^{\infty} \left(1 - \frac{\ell_\mathrm{N}(R)}{\ell_\mathrm{N}(R) + \delta\, \ell_\mathrm{N}(t)}\right) t\, (1 - v(t)) dt, \tag{41}$$

$$I_\mathrm{S} = \int_{2\,R_\mathrm{I}}^{\infty} \left(1 - \left(1 + \frac{\delta\, \frac{P_\mathrm{S}}{P_\mathrm{O}}\, L_W \ell_\mathrm{L}(t)}{\ell_\mathrm{N}(R_0)\, N_\mathrm{L}}\right)^{-N_\mathrm{L}}\right) e^{-(\beta_\mathrm{B} t + p_\mathrm{B})}\, t\, dt, \tag{42}$$

$$I_{\overline{\mathrm{S}}} = \int_{2R_\mathrm{I}}^{\infty} \frac{\delta\, \frac{P_\mathrm{S}}{P_\mathrm{O}} L_\mathrm{W} \ell_\mathrm{N}(t)}{\ell_\mathrm{N}(R) + \delta\, \frac{P_\mathrm{S}}{P_\mathrm{O}} L_\mathrm{W} \ell_\mathrm{N}(t)} \left(1 - e^{-(\beta_\mathrm{B} t + p_\mathrm{B})}\right) t\, dt. \tag{43}$$

Proof. For a given BS distance R_0, the proof for $\mathbb{P}[\gamma_\mathrm{L}(R_0) > \delta]$ is provided in Appendix C, while the proof for $\mathbb{P}[\gamma_\mathrm{N}(R_0) > \delta]$ is carried out along the lines of (50) in Appendix B. Averaging over R_0 by applying Lemmas 1 and 2 yields (34) and (39), respectively. □

Finally, the SIR-coverage probability of a *typical* indoor user at distance r, $0 < r \le R_\mathrm{I}$, which experiences LOS- and NLOS macro BSs, can be expressed as

$$P_c(\delta|r) = \eta P_{c,\mathrm{S}}(\delta|r) + (1-\eta)(A_\mathrm{L} P_{c,\mathrm{L}}(\delta) + (1 - A_\mathrm{L}) P_{c,\mathrm{N}}(\delta)), \tag{44}$$

where η denotes the small cell occupation probability and A_L is the likelihood that the user associates with a LOS macro BS, as derived in (10).

The SIR-coverage probabilities in Theorems III.1 and III.2 exhibit a negative exponential scaling with the small cell BS density μ_S and the outdoor BS density μ_O. The term μ_S encompasses the building density λ_B as well as the small cell occupation probability η. While η only affects μ_S in (29), (34), and (39), λ_B also impacts the parameter β_B as well as the functions ℓ_N and $v(t)$. Thus, λ_B effectively alters all four terms I_L, I_N, I_S and $I_{\overline{\mathrm{S}}}$.

A second observation is that the SIR-coverage probabilities are only dependent on the ratio between the transmit powers P_S and P_O, rather than their absolute value.

The expressions for the SIR-coverage probability in Theorems III.1 and III.2 are not obtained in a closed form, but involve the evaluation of the one-fold integrals I_L, I_N, I_S and $I_{\overline{\mathrm{S}}}$ in Theorem III.1 and a three-fold integration in Theorem III.2. Due to the convenient structure of these terms, there is no need for applying tedious Monte Carlo methods. Their numerical computation is achieved by modern computer software such as *Maple* and *Mathematica*.

The integrals I_L, I_N, I_S and $I_{\overline{\mathrm{S}}}$ correspond to the individual SIR terms if only small cell BSs in neighboring or non-neighboring buildings, or outdoor BSs in LOS or NLOS were present as interferers. In order to get a better intuition on these terms, we consider two special cases.

Special case 1: No buildings ($\lambda_\mathrm{B} = 0$): In this case, we assume that only the building at the origin is maintained. Consequently, $\mu_\mathrm{S} = 0$, i.e., there are no small cells, and the coverage term $P_{c,\mathrm{S}}$ in (44) vanishes. On the other hand, the LOS probability $v(t) = 1$, which implies that $A_\mathrm{L} = 1$. Hence, (44) simplifies to $P_c(\delta|r) = P_{c,\mathrm{L}}(\delta)$. Furthermore, $I_\mathrm{N} = 0$ in Theorem III.2, and $f_\mathrm{L}(\cdot)$ in (7) amounts to the standard distance distribution of a PPP with an exclusion region of radius R_I around the origin [22]. Note that the coverage probability $P_c(\delta|r)$ is still dependent on the macro BS density μ_O, since the exclusion region does not scale with μ_O. Moreover, $P_c(\delta|r)$ is larger than zero due to the non-singular path loss model and the guard region [21].

Special case 2: No small cells ($\eta = 0$): In this case, (44) simplifies to $P_c(\delta|r) = A_\mathrm{L} P_{c,\mathrm{L}}(\delta) + (1 - A_\mathrm{L}) P_{c,\mathrm{N}}(\delta)$. The integrals for I_S in (37) and **??** are not taken into account in (34) and (39), since $\mu_\mathrm{S} = 0$. Then, the coverage probability only depends on the building size R_I, the building density λ_B and the macro BS density μ_O.

IV. Numerical Evaluation

In this section, the performance of a typical user at the edge of a building, i.e., $r = R_\mathrm{I}$, is evaluated numerically. At this location, *[Assoc-Asmp-1]*, *[Assoc-Asmp-2]* and *[VBl-Approx]* are expected to perform worst.

A. Parameters for Evaluation

We evaluate two 3GPP compliant scenarios [12][30]. The two setups refer to a sparse outdoor BS deployment with large transmit power and a dense outdoor BS deployment with low transmit power. In the first setup, we assume the outdoor BSs to be represented by macro BSs that transmit with a power of $46\,\mathrm{dBm}$ and are distributed with a spatial density of $\mu_{\mathrm{O}} = 4.61 \cdot 10^{-6}\,\mathrm{m}^2$, according to an inter-site distance of $500\,\mathrm{m}$. In the second setup, the outdoor BS are considered to be pico BSs with a transmit power of $24\,\mathrm{dBm}$ and are separated by a distance of $80\,\mathrm{m}$ on average, according to $\mu_{\mathrm{O}} = 1.804\,10^{-4}\,\mathrm{m}^{-2}$. In both scenarios, the indoor small cell BSs are represented by femto BSs with a transmit power of $20\,\mathrm{dBm}$. The buildings are assumed to attenuate the signal by a building penetration loss of $L_{\mathrm{B}} = 20\,\mathrm{dB}$. Following building statistics in [7] that were evaluated for Chicago and Manhattan, the average building radius is specified as $R_{\mathrm{I}} = 15\,\mathrm{m}$. For both LOS and NLOS wall penetration losses, we investigate $L_{\mathrm{L}} = \{0, 20\}\,\mathrm{dB}$ and $L_{\mathrm{N}} = \{0, 20\}\,\mathrm{dB}$, thus including the cases where the outer wall of the target building offers no isolation between indoor- and outdoor environment. The path loss constants and exponents in (3), (4), and (6) are referred from [12][30], and are summarized in Table I. For LOS links, we consider three different values $N_{\mathrm{L}} = \{1, 2, 3\}$ of the Nakagami-m parameter. Note that $N_{\mathrm{L}} = 1$ corresponds to Rayleigh fading.

For the validation of *[Assoc-Asmp-1]* and *[Assoc-Asmp-2]* from Section II-C, *[VBl-Approx]* from Section II-D and *[Int-Asmp]* from Section III, Monte Carlo simulations are carried out. BSs and buildings are distributed over a field of $5000 \times 5000\,\mathrm{m}$. The simulations are performed with a bandwidth of $10\,\mathrm{MHz}$, a noise power density of $-174\,\mathrm{dBm}$ as referred from [31], and a receiver noise figure of $9\,\mathrm{dB}$. The results are assessed by averaging over 10^5 network and building realizations.

TABLE I: Parameters for numerical evaluation.

Parameter	Value
Carrier frequency	$2\,\mathrm{GHz}$ [30][12]
Bandwidth	$10\,\mathrm{MHz}$ [30][12]
Macro total transmit power	$46\,\mathrm{dBm}$ [40 W][30][12]
Macro inter-site distance	$500\,\mathrm{m}$; $\mu_{\mathrm{O}} = 4.61 \cdot 10^{-6}\ \mathrm{m}^{-2}$ [30][12]
LOS path loss	$\ell_{\mathrm{L}}(R_{[\mathrm{km}]}) = 103.4 + 24.2\log_{10}(R)$ [30][12, Model 2]
NLOS path loss	$\ell_{\mathrm{N}}(R_{[\mathrm{km}]}) = 131.1 + 42.8\log_{10}(R)$ [30][12, Model 2]
Pico total transmit power	$24\,\mathrm{dBm}$ [250 mW] [12][30]
Inter-pico distance	$80\,\mathrm{m}$; $\mu_{\mathrm{O}} = 1.804\,10^{-4}\,\mathrm{m}^{-2}$ [30]
LOS path loss	$\ell_{\mathrm{L}}(R_{[\mathrm{km}]}) = 103.8 + 20.9\log_{10}(R)$ [30][12]
NLOS path loss	$\ell_{\mathrm{N}}(R_{[\mathrm{km}]}) = 145.4 + 37.5\log 10(R)$ [30][12]
Femto total transmit power	$20\,\mathrm{dBm}$ [100 mW][32]
Indoor path loss	$p_{\mathrm{I}}(R) = 38.46 + 20\log_{10}(R)$ [12][30]
Radius of building area	$R_{\mathrm{I}} = 15$ m (conf. [7])
Building penetration loss	$L_{\mathrm{B}} = 20$ dB
Indoor-to-outdoor pen. loss	$L_{\mathrm{W}} = 20$ dB [30][12]
NLOS wall penetration loss	$L_{\mathrm{N}} = \{0, 20\}$ dB [30][12]
LOS wall penetration loss	$L_{\mathrm{L}} = \{0, 20\}$ dB
Receiver noise figure	$9\,\mathrm{dB}$ [12][30]
Noise power density	$-174\,\mathrm{dBm/Hz}$ [31]

B. Average Number of Visible BSs and Association Probability

Fig. 2 shows the average number of outdoor BSs in LOS over the indoor area coverage ratio p_{I} for macro- and pico BS densities of $\mu_{\mathrm{O}} = 4.61 \cdot 10^{-6}\,\mathrm{m}^2$ and $\mu_{\mathrm{O}} = 1.804\,10^{-4}\,\mathrm{m}^{-2}$ respectively. The curves are obtained by evaluating (17). As expected, the average number of outdoor BSs in LOS decreases with a larger indoor area coverage p_{I}. Remarkably, the average number of pico BSs in LOS falls below one only for $p_{\mathrm{I}} \geq 0.7$. In Section II-A, we obtained $p_{\mathrm{I}} = 0.46$ and $p_{\mathrm{I}} = 0.42$ for Manhattan and Chicago, concluding that in any practical urban environment with a 3GPP compliant pico BS deployment, on average the user will experience at least one BS in LOS. On the other hand, the average number of LOS macro BS is always lower than one. The results achieve a remarkably accurate fit with the simulations, verifying the accuracy of *[VBl-Approx]*.

For comparison, we also carry out simulations with macro- and pico-LOS functions from the 3GPP standard. In particular, we apply the functions from [30] and [12, Case 1], which are defined as

$$v(R_{[\mathrm{km}]}) = \min(0.018/R, 1)(1 - \exp(-R/0.063)) + \exp(-R/0.063) \tag{45}$$

for an urban macro BS topology, and

$$v(R_{[\mathrm{km}]}) = 0.5 - \min(0.5, 5\exp(-0.156/R)) + \min(0.5, 5\exp(-R/0.03)) \tag{46}$$

for a pico BS setup. The results are also depicted in Fig. 2. It is observed that the results do not vary with p_{I}, since the 3GPP LOS functions are not dependent on the indoor area coverage. Thus, they are only valid for a specific urban topology. In both macro- and pico scenarios, the average number of outdoor BSs in LOS is larger than one. Compared to the results from (17), in the pico case, equality is obtained at $p_{\mathrm{I}} = 0.38$, while the values are consistently larger in the macro case.

Fig. 3 depicts the probabilities for a user in a typical building to be associated with an outdoor BS in NLOS as well as the likelihood to observe at least one BS in LOS and to be attached to it. Results are shown for LOS and NLOS wall penetration losses of $L_{\mathrm{L}} = \{0, 20\}\,\mathrm{dB}$ and $L_{\mathrm{N}} = \{0, 20\}\,\mathrm{dB}$. The curves are obtained by evaluating (8), (10) and (14) for both macro- and pico scenarios, respectively.

It is observed that for an NLOS wall penetration loss of $L_{\mathrm{N}} = 20\,\mathrm{dB}$ (conf. Fig. 3b) and an indoor area coverage of $p_{\mathrm{I}} = 0.2$, the user associates with an NLOS macro BS in 70% of the cases, while in the pico scenarios (conf. Fig. 3d), it almost surely associates with a pico BS in LOS. As expected, in both macro- and the pico scenarios, the probability to experience at least one outdoor BS in LOS decreases with larger values of p_{I}. Remarkably, in the presence of at least

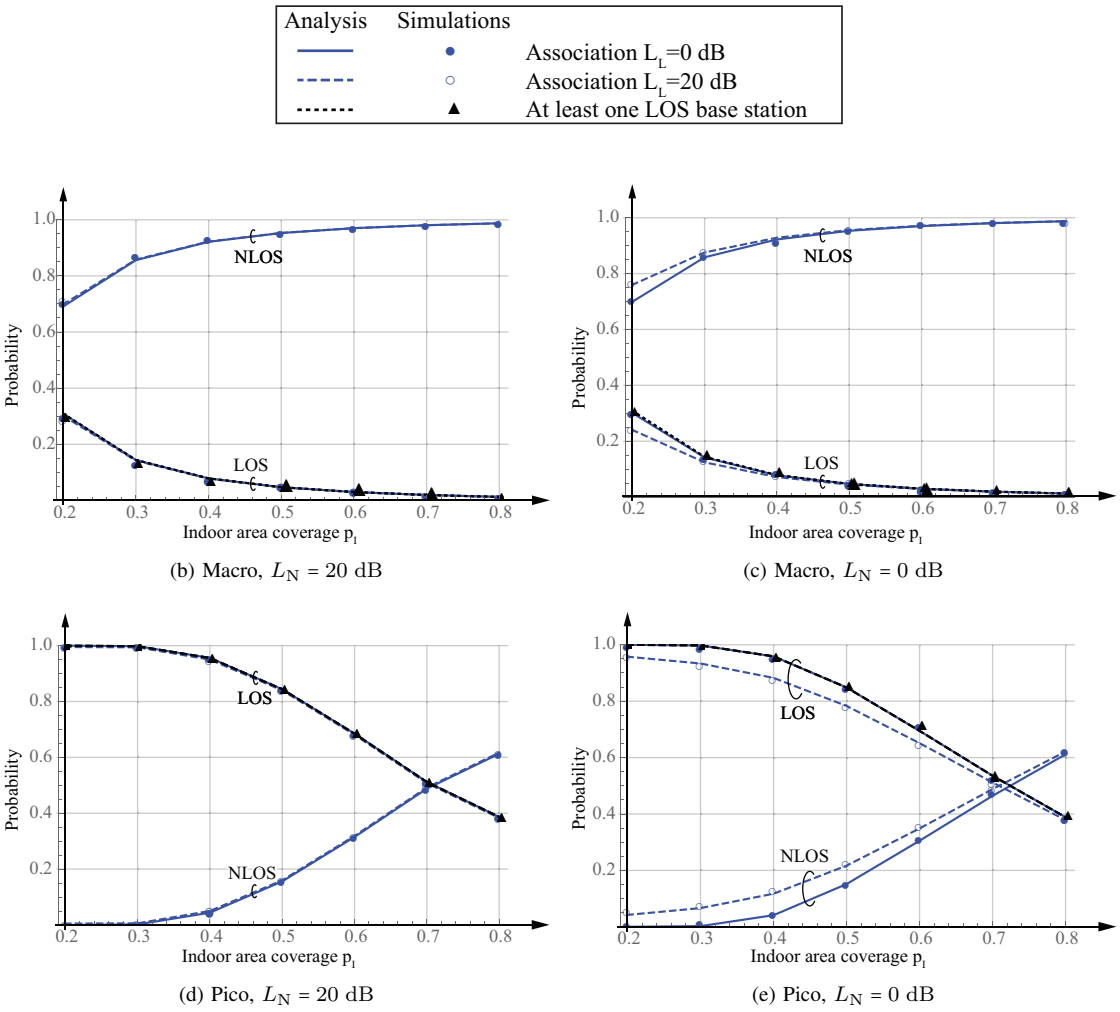

(b) Macro, L_{N} = 20 dB

(c) Macro, L_{N} = 0 dB

(d) Pico, L_{N} = 20 dB

(e) Pico, L_{N} = 0 dB

Fig. 3: User association probabilities for outdoor BS in LOS and NLOS and probability that user observes at least one outdoor BS in LOS (dotted curve) over indoor coverage ratio.

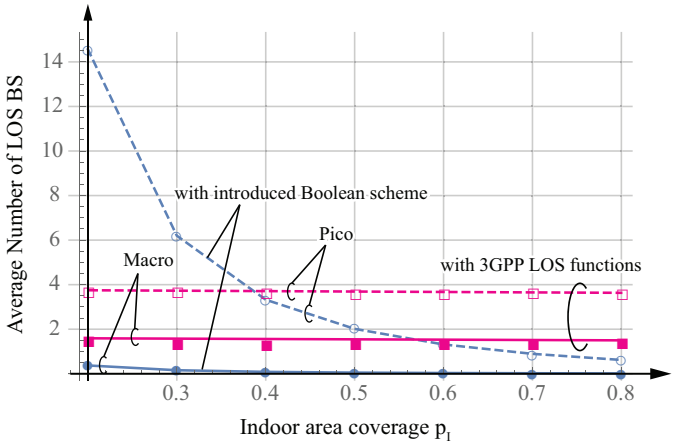

Fig. 2: Average number of outdoor BSs in LOS versus indoor area coverage ratio p_{I}. Curves show analytical results as obtained with the Boolean scheme, and results from simulations with LOS functions from 3GPP.

one outdoor BS in LOS, the user *almost surely* associates with a LOS BS. Comparing the results for L_{N} = 0 dB and the L_{N} = 20 dB, the LOS association probabilities are similar when L_{L} = 0 dB, but smaller for L_{N} = 0 dB and L_{L} = 20 dB. This result is remarkable in view of the NLOS propagation characteristics. Despite suffering from considerable attenuation due to blockages, the final impact of the wall penetration loss is non-negligible for the likelihood of association with an NLOS BS. In other words, by lowering L_{N}, the NLOS BSs become more competitive for being the desired BS. The effect is most prominent in the pico scenarios and L_{N} = 0 dB (conf. Fig. 3e). The gap between L_{L} = 0 dB and L_{L} = 20 dB closes for larger values of p_{I}, since the growing attenuation due to blockages eventually outweighs the effect of L_{L}. The results from the Monte Carlo simulations accurately fit with the analytical values, thus verifying *[VBl-Approx]*.

C. Spectral Efficiency

In the next step, we investigate the spectral efficiency. It yields an upper bound of the average data rate that can be supported in a cellular network per bandwidth, and is defined

as $\tau(r) = \mathbb{E}_{\gamma(r)}[\log_2(1+\gamma(r))]$. Observing the fact that the SIR-coverage probability corresponds to the Complementary Cumulative Distribution Function (CCDF) of the SIR, and applying the truncated Shannon formula from [31, Annex A] (neglecting the implementation losses for simplicity), we can reformulate $\tau(r)$ as

$$\tau(r) = \frac{1}{\log(2)} \int_{\delta_{\min}}^{\delta_{\max}} \frac{P_c(\delta|r)}{1+\delta} d\delta, \tag{47}$$

with $P_c(\delta|r)$ from (44), $\delta_{\max} = 2^6 - 1$, referring to 64-Quadrature Amplitude Modulation (QAM), which is the highest modulation order in the current LTE-A standard, and $\delta_{\min} = 0.1$ according to [31, Annex A]. Note that a system with link adaptation will require a different notion of *coverage* then the one defined in Section III-B, e.g., $\mathbb{P}[\gamma_s(r) > \delta_{\min}]$.

Fig. 4 depicts the spectral efficiency $\tau(r)$ in $[\mathrm{bit/s/Hz}]$ for various indoor coverage probabilities p_{I}, occupation probabilities $\eta = \{0.2, 0.5, 0.8\}$, Nakagami-m parameters $N_{\mathrm{L}} = \{1, 2, 3\}$, as well as LOS and NLOS wall penetration losses $L_{\mathrm{L}} = \{0, 20\}\,\mathrm{dB}$ and $L_{\mathrm{N}} = \{0, 20\}\,\mathrm{dB}$. The figure also shows the performance *without buildings* (*special case 1* in Section III-B) and without small cells, i.e., $\eta = 0$ (*special case 2* in Section III-B).

A first general observation is that the results for Rayleigh fading along the LOS links, i.e., $N_{\mathrm{L}} = 1$, closely approximate the curves for $N_{\mathrm{L}} = \{2, 3\}$. This outcome follows findings in [2] and [5], where results turned out to be similar for distinct fading distributions, as long as these distributions have the same mean. The authors in [5] argue that it arises from the spatial averaging inherent to stochastic geometry. Minor deviations from the results with Rayleigh fading only occur in the pico scenario for $L_{\mathrm{L}} = 0\,\mathrm{dB}$, as indicated by the enlarged cut-outs in Figures 4d and 4e. They mainly originate from the extensive presence of pico BSs in LOS.

Fig. 4b shows the results for scenarios, where the outdoor BSs are represented by macro BSs and $L_{\mathrm{N}} = 20\,\mathrm{dB}$. It is observed that for $\eta = 0.2$ as well as $\eta = 0.5$ and $L_{\mathrm{L}} = 20$ dB, the performance monotonically decreases when increasing the indoor area coverage p_{I}. Remarkably, this stands in contrast to the observations in [15][22], where it was found that a larger building density effectively provides a safeguard against the interference. In Fig. 4b, this protection effect can be observed, e.g., for $\eta = 0$, where the spectral efficiency monotonically increases with larger p_{I}. The decreasing performance for $\eta = 0.2$ and $\eta = 0.5$ is mainly caused by the decreasing likelihood of being associated with a macro BS in LOS (conf. Fig. 3b) as well as the low performance that is achieved when the user is associated with an NLOS BS. It stems from the fact that for large values of p_{I}, the amount of interfering small cell BSs effectively increases. Due to the large building density, these small cell BS are most likely located in non-neighboring buildings, hence experiencing NLOS conditions. Then, the desired as well as the interfering signals fade according to the same law, while the number of interferers is growing. Hence, taking into account small cell BSs in neighboring buildings *annihilates the protecting effect of the blockages against the interference*.

A second observation is that for all scrutinized values of η, the gap between $L_{\mathrm{L}} = 0\,\mathrm{dB}$ and $L_{\mathrm{L}} = 20\,\mathrm{dB}$ closes at a large indoor area coverage p_{I}. The two main sources of the gap are (i) user that are associated with an NLOS macro BS, and experience interference from small cell BS in *neighboring* buildings with a decreasing likelihood for larger p_{I}, and (ii) small cell BS associated users that experience interference from LOS macro BSs with a lower likelihood for greater p_{I}. The claim that this effect is mainly related to small cell association and small cell interference is verified by the fact that it is hardly visible for $\eta = 0$. Remarkably, for $\eta = 0$ and $p_{\mathrm{I}} = 0$, the $L_{\mathrm{L}} = 0\,\mathrm{dB}$ case achieves a better performance than $L_{\mathrm{L}} = 20\,\mathrm{dB}$. The result stems from the fact that if the user is associated with a macro BS in LOS, this BS is highly likely the only one in LOS.

Lastly, we observe that for $\eta > 0$, the rate monotonically increases with increasing η. For $\eta = 0.8$, the performance grows for $L_{\mathrm{L}} = 0\,\mathrm{dB}$ and increasing p_{I}, while remaining almost constant for $L_{\mathrm{L}} = 20\,\mathrm{dB}$. Interestingly, compared to $\eta = 0.2$ and $\eta = 0.5$ the performance does not degrade with larger p_{I}. This result indicates that the performance of a user in a small cell-occupied building is mainly determined by the interfering macro BSs in LOS rather than the interference from small cell BSs in neighboring and non-neighboring buildings.

Fig. 4c depicts results for the same macro scenario, except that the wall loss of the NLOS signals is considered to be $L_{\mathrm{N}} = 0\,\mathrm{dB}$ instead of $L_{\mathrm{N}} = 20\,\mathrm{dB}$. On first sight, the spectral efficiency values exhibit similar trends as observed for $L_{\mathrm{N}} = 20\,\mathrm{dB}$. Nevertheless, three peculiarities of the $L_{\mathrm{N}} = 0\,\mathrm{dB}$ case are identified. First, we observe that for $\eta = 0.2$, $L_{\mathrm{L}} = 20$ dB and $L_{\mathrm{L}} = 0$ dB yield a smaller gap than for $L_{\mathrm{N}} = 20$ dB. The result mainly stems from the performance improvement of an NLOS macro BS associated user in the low p_{I} regime. In this regime, the interference is dominated by macro BSs in LOS as well as small cell BSs in neighboring buildings. Hence, although setting $L_{\mathrm{N}} = 0$ dB increases both desired as well as interfering signal strengths from NLOS macro BSs, it mainly improves the relevance of the desired BS. Moreover, according to Theorem 1, it decreases the average distance of the desired NLOS macro BS. Thus, a similar performance between $L_{\mathrm{L}} = 0$ dB and $L_{\mathrm{L}} = 20$ dB scenarios or $L_{\mathrm{N}} = 0$ dB and $L_{\mathrm{N}} = 20$ dB scenarios does not necessarily lead to the conclusion that the performance is determined by a single type of BS, i.e., either LOS or NLOS. In the high p_{I} regime, similar to the $L_{\mathrm{N}} = 20$ dB scenarios, the interference from small cell BSs in non-neighboring buildings comes into effect. Since those are also assumed to experience $L_{\mathrm{N}} = 0$ dB, the performance is similar to $L_{\mathrm{N}} = 20$ dB.

The second important observation compared to $L_{\mathrm{N}} = 20$ dB is that the rate at $\eta = 0.8$ and $p_{\mathrm{I}} = 0.2$ is slightly lower for $L_{\mathrm{N}} = 0$ dB. Users in small-cell occupied buildings now experience strong interference not only from macro BSs in LOS but also from those in NLOS. Remarkably, for $L_{\mathrm{L}} = 20$ dB the rate increases with increasing p_{I}. Eventually, at $p_{\mathrm{I}} = 0.8$ almost the same rate as in the $L_{\mathrm{N}} = 20$ dB case is achieved. This result indicates that in the high p_{I} regime, L_{N} has a minor impact on the interference than the building blockage.

In the next step, we investigate scenarios, where the outdoor BS are formed by densely deployed pico BSs and $L_{\mathrm{N}} = 20\,\mathrm{dB}$.

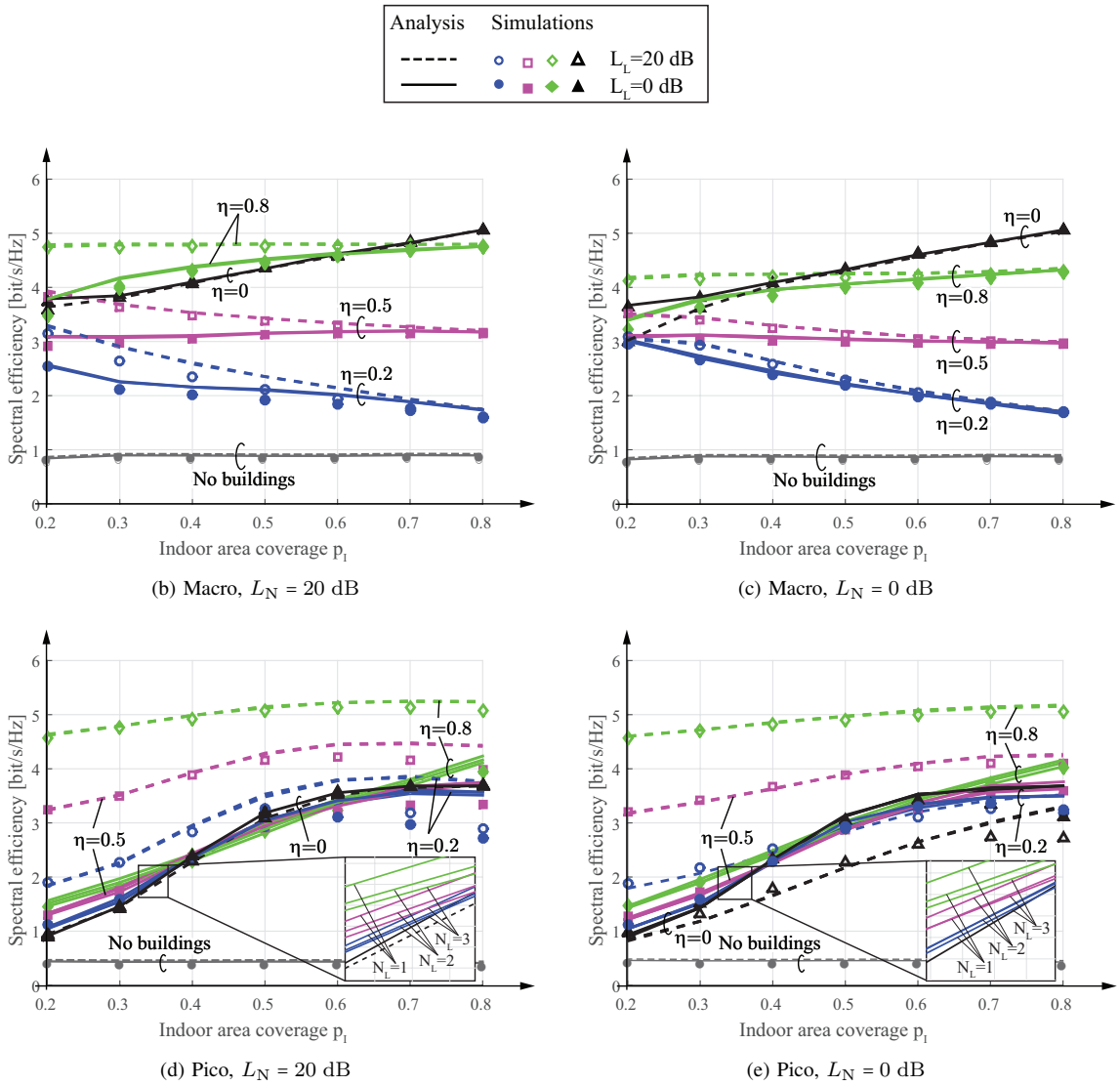

(b) Macro, L_{N} = 20 dB

(c) Macro, L_{N} = 0 dB

(d) Pico, L_{N} = 20 dB

(e) Pico, L_{N} = 0 dB

Fig. 4: Spectral efficiency [bit/s/Hz] over indoor area coverage p_{I} for various wall penetration losses $L_{\mathrm{N}} = \{0, 20\}$ dB, $L_{\mathrm{L}} = \{0, 20\}$ dB and occupation probabilities $\eta = \{0.2, 0.5, 0.8\}$. Dashed and solid lines refer to analytical results. Plot markers denote simulation results. Results are shown for different values of the Nakagami-m fading $N_{\mathrm{L}} = \{1, 2, 3\}$.

Reconsidering the results from Fig. 3, in such scenarios, an indoor user in a building without small cell BS is highly likely to experience and associate with a pico BS in LOS. Compared to the macro scenarios, this leads to considerably different dynamics between indoor coverage ratio p_{I} and spectral efficiency τ, as shown in Figures 4d and 4e, and explained in the following.

The first observation is that there is a large gap between the rate for L_{L} = 20 dB and L_{L} = 0 dB, in particular in the case of η = 0.8. Remarkably, as opposed to the macro BS scenarios, the gap does not vanish even for large values of p_{I}. Both observations confirm the conjecture in Section IV-B that the performance is largely dominated by pico BSs in LOS.

In the low p_{I} regime, the spectral efficiency increases with larger indoor area coverage p_{I} for all scrutinized values of η and both L_{L} = 20 dB and L_{L} = 0 dB. The improvement results from the buildings acting as a safeguard against the interference in the sense that they increase the likelihood of a BS being in LOS, thus effectively decreasing the amount of LOS interferers. In the high p_{I} regime, the performance for L_{L} = 20 dB and all values of η, as well as for L_{L} = 0 dB and η = 0.2 reaches a maximum and then degrades again. Intuitively, this maximum is achieved when only a single BS in LOS is present. Further increasing p_{I} leads into a regime of decreasing spectral efficiency, where users are mainly associated with an NLOS pico BS. According to Fig. 3d, at p_{I} = 0.8, more then 60% of the pico-associated users have their desired pico BS in NLOS.

A second distinct result is that for $p_{\mathrm{I}} > 0.4$ and L_{L} = 0 dB, the largest investigated occupation ratio η = 0.8 achieves the worst performance. It stems from the fact that the performance is mainly determined by users in a small cell occupied building that experience large interference from the LOS BSs. In the high p_{I} regime and L_{L} = 0 dB, low occupation ratios $\eta = \{0, 0.2, 0.5\}$ are again outperformed by η = 0.8, since the large building density blocks the LOS BSs and the case where a user

associates with an NLOS pico BS becomes more prominent.

Similar to the macro scenarios, in the next step, we drop L_{N} from 20 dB to 0 dB. The results are depicted in Fig. 4e. In comparison to L_{N} = 20 dB, the first observation is that the maxima of the spectral efficiency in the high indoor area coverage regime are no longer present. This result is remarkable in view of the larger likelihood to associate with a pico BS in NLOS (conf. Fig. 3e). Similar to the low p_{I} regime in the macro scenarios, it stems from the fact that L_{N} = 0 dB predominantly favors the desired BS in NLOS.

The second main difference to the L_{N} = 20 dB scenarios appears for a low occupation probability p_{I} = 0.2 and large indoor coverage ratios p_{I}, where the gap between L_{L} = 0 dB and L_{L} = 20 dB vanishes. Again, the drop of L_{N} puts the NLOS BSs in a more favorable state against the LOS BSs.

In the last step, we compare the analytically obtained spectral efficiencies in Fig. 4 against results from Monte Carlo simulations. It is seen that overall the results closely resemble the simulations, thus verifying the validity of the two association assumptions (*[Assoc-Asmp-1]*, *[Assoc-Asmp-2]*) as well as the *virtual building* approximation (*[VBl-Approx]*) and the conjecture of an interference limited network (*[Int-Asmp]*). In most cases, the results slightly overestimate the actual performance, which is a consequence of overestimating the SIR due to *[VBl-Approx]*. The protective effect of the virtual building is most prominent in the pico scenarios, in particular for L_{N} = 20 dB and large values of p_{I}. For L_{N} = 0 dB and low values of p_{I}, the analytical results tend to underestimate the actual performance. This mainly originates from *[Assoc-Asmp-2]*, which forces users in a small cell occupied building to associate with this small cell BS, although a larger SIR would be achieved by associating with an outdoor BS.

V. Conclusions

In this work, we introduced a framework for evaluating the downlink performance of a typical indoor user in urban two-tier heterogeneous mobile networks. We derived convenient expressions for the SIR-coverage probability and average spectral efficiency, and carried out numerical evaluations with 3GPP compliant macro- and pico BS deployments. In the macro scenarios, we observed that, contrary to previous work, a growing number of small cell BSs can pale the effect of the safeguard against the interference. In the pico scenarios, the safeguard reappears again. In contrast to prior work, it is established by the blockage density rather than the blockage attenuation. The interference protection results in a performance maximum at a certain indoor coverage ratio, where only a single pico BS is left in LOS. The wall penetration losses of LOS and NLOS signals were observed to have the strongest impact in the low indoor area coverage regime. A small wall loss of the NLOS signals significantly increases the likelihood of the strongest NLOS BS to become the desired BS. A low attenuation of the LOS signals makes LOS outdoor BSs the major source of interference for small cell-associated users. The high indoor area coverage regime is dominated by the attenuation due to building blockages. Remarkably, we observed that even if the difference between results with distinct wall penetration losses is almost negligible, the values may arise from entirely different dynamics between the wall penetration losses and the indoor area coverage. Lastly, the results from Monte Carlo simulations showed an accurate fit with the analytical results, thus confirming the accuracy of our assumptions. The remaining deviations were identified to stem from the restrictive user association policies. It is our hope that this paper raises awareness on the dynamics and challenges imposed by the indoor-outdoor partitioning in an urban environment. Our future work is directed towards incorporating further physical aspects such as reflections and correlations among blockages, as well as scrutinizing the typical outdoor user.

Appendix A
Proof of Lemma 1

The proof is derived along the lines of [27, Appendix B] by excluding BS from a ball of radius R_{I} around the user. A user is associated with a macro BS in LOS if and only if it has a BS in LOS and its path loss is smaller than the path loss from the closest NLOS BS. Let d_{L} and d_{N} denote the distance from the typical user to the nearest BS in Φ_{L} and Φ_{M}, respectively. Then,

$$\begin{aligned} A_{\mathrm{L}} &= B_{\mathrm{L}}\,\mathbb{P}\left[\ell_{\mathrm{L}}(d_{\mathrm{L}}) > \ell_{\mathrm{N}}(d_{\mathrm{N}})\right] \\ &= B_{\mathrm{L}} \int_{R_{\mathrm{I}}}^{\infty} \mathbb{P}[d_{\mathrm{N}} > \Psi(x)]\hat{f}_{\mathrm{L}}(x)dx, \end{aligned} \tag{48}$$

with B_{L} referring to the probability that the user has at least one macro BS in LOS and $\hat{f}_{\mathrm{L}}(x)$ is the PDF of the user's distance to its nearest LOS BS under the condition that is observes at least one BS in LOS. For the derivation of B_{L} and $\hat{f}_{\mathrm{L}}(x)$, the reader is referred to [15, Theorem 10]. The proof is completed by noting that

$$\begin{aligned} \mathbb{P}[d_{\mathrm{N}} > \Psi(x)] &= \mathbb{P}\left[\Phi_{\mathrm{N}} \cap \mathcal{B}(0,\Phi_{\mathrm{L}})\backslash\mathcal{B}(0,R_{\mathrm{I}}) = \varnothing\right] \\ &= e^{-2\pi\mu_{\mathrm{O}}\int_{R_{\mathrm{I}}}^{\Psi_{\mathrm{L}}(x)}(1-v(t))tdt} \end{aligned} \tag{49}$$

and plugging (49) into (48). The term $\mathcal{B}(x,r)$ denotes a ball of radius r that is centered at location x.

Appendix B
Proof of Theorem III.1

Applying (18), it follows from the independence of $G_{\mathrm{L},i}$, $G_{\mathrm{N},i}$, and $G_{\mathrm{I},i}$, the independence of Φ_{L}, Φ_{N} and Φ_{S}, and the fact that $G_{\mathrm{I},0}$ is a exponentially distributed RV that

$$\begin{aligned} P_{c,\mathrm{S}}(\delta|r) &= \mathbb{P}\left[\gamma_{\mathrm{S}}(r) > \delta|r\right] \\ &= \mathbb{E}\left[\exp\left(-\frac{\delta}{P_{\mathrm{S}}\ell_{\mathrm{I}}(r)}\Sigma_{\mathrm{L}}\right)\right]\mathbb{E}\left[\exp\left(-\frac{\delta}{P_{\mathrm{S}}\ell_{\mathrm{I}}(r)}\Sigma_{\mathrm{N}}\right)\right] \\ &\quad\cdot\mathbb{E}\left[\exp\left(-\frac{\delta}{P_{\mathrm{S}}\ell_{\mathrm{I}}(r)}\Sigma_{\mathrm{S}}\right)\right]\mathbb{E}\left[\exp\left(-\frac{\delta}{P_{\mathrm{S}}\ell_{\mathrm{I}}(r)}\Sigma_{\overline{\mathrm{S}}}\right)\right], \end{aligned} \tag{50}$$

with Σ_{L}, Σ_{N}, Σ_{S} and $\Sigma_{\overline{\mathrm{S}}}$ from (19)–(22), respectively. In the next step, the individual expectation terms in (50) are calculated.

$$\mathbb{E}\left[\exp\left(-\frac{\delta}{P_{\mathrm{S}}\,\ell_{\mathrm{I}}(r)}\Sigma_{\mathrm{L}}\right)\right]$$

$$= \mathbb{E}\left[\exp\left(-\frac{\delta}{P_{\mathrm{S}}\,\ell_{\mathrm{I}}(r)}\sum_{\substack{i:x_i\in\Phi_{\mathrm{L}}\\ \setminus\mathcal{B}(0,R_{\mathrm{I}})}} P_{\mathrm{O}}G_{\mathrm{L},i}\ell_{\mathrm{L}}(R_i)\right)\right]$$

$$\overset{(a)}{=} \mathbb{E}_{\Phi_{\mathrm{L}}}\left[\prod_{\substack{i:x_i\in\Phi_{\mathrm{L}}\\ \setminus\mathcal{B}(0,R_{\mathrm{I}})}}\left(1+\frac{\delta\,P_{\mathrm{O}}\,\ell_{\mathrm{L}}(R_i)}{P_{\mathrm{S}}\,\ell_{\mathrm{I}}(r)\,N_{\mathrm{L}}}\right)^{-N_{\mathrm{L}}}\right]$$

$$\overset{(b)}{=} \exp\left(-2\pi\mu_{\mathrm{O}}\int_{R_{\mathrm{I}}}^{\infty}\left(1-\left(1+\frac{\delta\,P_{\mathrm{O}}\,\ell_{\mathrm{L}}(t)}{P_{\mathrm{S}}\,\ell_{\mathrm{I}}(r)\,N_{\mathrm{L}}}\right)^{-N_{\mathrm{L}}}\right)\cdot t\,v(t)dt\right), \tag{51}$$

where (a) follows from the fact that $G_{\mathrm{L},i}$ are Gamma RVs with shape parameter N_{L} and scale parameter $1/N_{\mathrm{L}}$, and (b) follows from the probability generating functional of a PPP.

$$\mathbb{E}\left[\exp\left(-\frac{\delta}{P_{\mathrm{S}}\,\ell_{\mathrm{I}}(r)}\Sigma_{\mathrm{N}}\right)\right]$$

$$= \mathbb{E}\left[\exp\left(-\frac{\delta}{P_{\mathrm{S}}\,\ell_{\mathrm{I}}(r)}\sum_{\substack{j:x_j\in\Phi_{\mathrm{N}}\\ \setminus\mathcal{B}(0,R_{\mathrm{I}})}} P_{\mathrm{O}}G_{\mathrm{N},j}\ell_{\mathrm{N}}(R_j)\right)\right]$$

$$= \mathbb{E}_{\Phi_{\mathrm{N}}}\left[\prod_{\substack{j:x_j\in\Phi_{\mathrm{N}}\\ \setminus\mathcal{B}(0,R_{\mathrm{I}})}}\frac{P_{\mathrm{S}}\ell_{\mathrm{I}}(r)}{P_{\mathrm{S}}\ell_{\mathrm{I}}(r)+\delta\,P_{\mathrm{O}}\,\ell_{\mathrm{N}}(R_j)}\right]$$

$$= \exp\left(-2\pi\mu_{\mathrm{O}}\int_{R_{\mathrm{I}}}^{\infty}\left(1-\frac{P_{\mathrm{S}}\ell_{\mathrm{I}}(r)}{P_{\mathrm{S}}\ell_{\mathrm{I}}(r)+\delta\,P_{\mathrm{O}}\,\ell_{\mathrm{N}}(t)}\right)\cdot t(1-v(t))dt\right). \tag{52}$$

$$\mathbb{E}\left[\exp\left(-\frac{\delta}{P_{\mathrm{S}}\ell_{\mathrm{I}}(r)}\Sigma_{\mathrm{S}}\right)\right]$$

$$= \mathbb{E}\left[\exp\left(-\frac{\delta}{\ell_{\mathrm{I}}(r)}\sum_{\substack{k:X_k\in\Phi_{\mathrm{S}}\\ \setminus\mathcal{B}(0,2R_{\mathrm{I}})}} S_k\,G_{\mathrm{L},k}L_W\ell_{\mathrm{L}}(R_k)\right)\right]$$

$$\overset{(a)}{=} \mathbb{E}_{\Phi_{\mathrm{S}}}\left[\prod_{\substack{k:X_k\in\Phi_{\mathrm{S}}\\ \setminus\mathcal{B}(0,2R_{\mathrm{I}})}} 1+\left(-1+\left(1+\frac{\delta\,L_W\ell_{\mathrm{L}}(R_k)}{\ell_{\mathrm{I}}(r)\,N_{\mathrm{L}}}\right)^{-N_{\mathrm{L}}}\right)\cdot e^{-(\beta_{\mathrm{B}}R_k+p_{\mathrm{B}})}\right]$$

$$= \exp\left(-2\pi\mu_{\mathrm{S}}\int_{2\,R_{\mathrm{I}}}^{\infty}\left(1-\left(1+\frac{\delta\,L_W\ell_{\mathrm{L}}(t)}{\ell_{\mathrm{I}}(r)\,N_{\mathrm{L}}}\right)^{-N_{\mathrm{L}}}\right)\cdot e^{-(\beta_{\mathrm{B}}t+p_{\mathrm{B}})}\,t\,dt\right). \tag{53}$$

where (a) results from S_k being Bernoulli RVs with parameters $\exp(-\beta_{\mathrm{B}}R_j - p_{\mathrm{B}})$.

$$\mathbb{E}\left[\exp\left(-\frac{\delta}{P_{\mathrm{S}}\ell_{\mathrm{I}}(r)}\Sigma_{\overline{\mathrm{S}}}\right)\right]$$

$$= \mathbb{E}\left[\exp\left(-\frac{\delta}{\ell_{\mathrm{I}}(r)}\sum_{\substack{k:X_k\in\Phi_{\mathrm{S}}\\ \setminus\mathcal{B}(0,2R_{\mathrm{I}})}} \overline{S}_k G_{\mathrm{N},k}L_W\ell_{\mathrm{N}}(R_k)\right)\right]$$

$$= \mathbb{E}_{\Phi_{\mathrm{S}}}\left[\prod_{\substack{k:X_k\in\Phi_{\mathrm{S}}\\ \setminus\mathcal{B}(0,2R_{\mathrm{I}})}} 1-\frac{\delta L_{\mathrm{W}}\ell_{\mathrm{N}}(R_k)\left(1-e^{-(\beta_{\mathrm{B}}R_k+p_{\mathrm{B}})}\right)}{\ell_{\mathrm{I}}(r)+\delta L_{\mathrm{W}}\ell_{\mathrm{N}}(R_k)}\right]$$

$$= \exp\left(-2\pi\mu_{\mathrm{S}}\int_{2\,R_{\mathrm{I}}}^{\infty}\frac{\delta L_{\mathrm{W}}\ell_{\mathrm{N}}(t)}{\ell_{\mathrm{I}}(r)+\delta L_{\mathrm{W}}\ell_{\mathrm{L}}(t)}\cdot\left(1-e^{-(\beta_{\mathrm{B}}t+p_{\mathrm{B}})}\right)tdt\right). \tag{54}$$

Plugging (51)–(54) into (50) completes the proof.

Appendix C
Proof of Theorem III.2

$$P_{c,\mathrm{L}}(\delta|R_0) = \mathbb{P}\left[G_0 > \frac{\delta}{P_{\mathrm{O}}\,\ell_{\mathrm{L}}(R_0)}\left(\Sigma'_{\mathrm{L}}+\Sigma'_{\mathrm{N}}+\Sigma_{\mathrm{S}}+\Sigma_{\overline{\mathrm{S}}}\right)\right] \tag{55}$$

$$\overset{(a)}{\approx} 1-\mathbb{E}\left[\left(1-\exp\left(-\frac{\nu_{\mathrm{L}}\,\delta}{P_{\mathrm{O}}\ell_{\mathrm{L}}(R_0)}\cdot\left(\Sigma'_{\mathrm{L}}+\Sigma'_{\mathrm{N}}+\Sigma_{\mathrm{S}}+\Sigma_{\overline{\mathrm{S}}}\right)\right)\right)^{N_{\mathrm{L}}}\right]$$

$$\overset{(b)}{=} \sum_{n=1}^{N_{\mathrm{L}}}(-1)^{n+1}\binom{N_{\mathrm{L}}}{n}\mathbb{E}\left[\exp\left(-\frac{n\,\nu_{\mathrm{L}}\,\delta}{P_{\mathrm{O}}\ell_{\mathrm{L}}(R_0)}\cdot\left(\Sigma'_{\mathrm{L}}+\Sigma'_{\mathrm{N}}+\Sigma_{\mathrm{S}}+\Sigma_{\overline{\mathrm{S}}}\right)\right)\right] \tag{56}$$

with Σ'_{L}, Σ'_{N}, Σ_{S} and $\Sigma_{\overline{\mathrm{S}}}$ from (21), (22), (25), and (26), $\nu_{\mathrm{L}} = N_{\mathrm{L}}(N_{\mathrm{L}}!)^{-1/N_{\mathrm{L}}}$, the approximation in (a) follows from [33, Lemma 6] and (b) is derived from the Binomial theorem and the assumption that N_{L} is an integer. The rest of the proof is carried out along the lines of (50) in Appendix B.

References

[1] Ericsson, "Ericsson mobility report," Nov. 2013. [Online]. Available: http://www.ericsson.com/mobility-report

[2] J. Andrews, F. Baccelli, and R. Ganti, "A tractable approach to coverage and rate in cellular networks," *IEEE Transactions on Communications*, vol. 59, no. 11, pp. 3122–3134, Nov. 2011.

[3] H. Dhillon, R. Ganti, F. Baccelli, and J. Andrews, "Modeling and analysis of K-tier downlink heterogeneous cellular networks," *IEEE Journal on Selected Areas in Communications*, vol. 30, no. 3, pp. 550–560, April 2012.

[4] C. Galiotto, N. K. Pratas, N. Marchetti, and L. Doyle, "A stochastic geometry framework for LOS/NLOS propagation in dense small cell networks," *CoRR*, vol. abs/1412.5065, 2014. [Online]. Available: http://arxiv.org/abs/1412.5065

[5] X. Zhang and J. G. Andrews, "Downlink cellular network analysis with multi-slope path loss models," *CoRR*, vol. abs/1408.0549, 2014. [Online]. Available: http://arxiv.org/abs/1408.0549

[6] M. Ding, P. Wang, D. López-Pérez, G. Mao, and Z. Lin, "Performance impact of LoS and NLoS transmissions in small cell networks," *CoRR*, vol. abs/1503.04251, 2015. [Online]. Available: http://arxiv.org/abs/1503.04251

[7] M. Kulkarni, S. Singh, and J. Andrews, "Coverage and rate trends in dense urban mmwave cellular networks," in *IEEE Global Commun. Conf. (GLOBECOM)*, Dec. 2014, pp. 3809–3814.

[8] T. A. Khan, A. Alkhateeb, and R. W. H. Jr., "Millimeter wave energy harvesting," *CoRR*, vol. abs/1509.01653, 2015. [Online]. Available: http://arxiv.org/abs/1509.01653

[9] M. Di Renzo, "Stochastic geometry modeling and analysis of multi-tier millimeter wave cellular networks," *IEEE Trans. Wireless Commun.*, vol. 14, no. 9, pp. 5038–5057, Sept 2015.

[10] W. Lu and M. Di Renzo, "Stochastic geometry modeling of cellular networks: Analysis, simulation and experimental validation," in *Proceedings of the 18th ACM International Conference on Modeling, Analysis and Simulation of Wireless and Mobile Systems*, ser. MSWiM '15. New York, NY, USA: ACM, 2015, pp. 179–188. [Online]. Available: http://doi.acm.org/10.1145/2811587.2811597

[11] F. Ademaj, M. Taranetz, and M. Rupp, "3gpp 3d mimo channel model: a holistic implementation guideline for open source simulation tools," *EURASIP Journal on Wireless Communications and Networking*, vol. 2016, no. 1, pp. 1–14, 2016. [Online]. Available: http://dx.doi.org/10.1186/s13638-016-0549-9

[12] 3rd Generation Partnership Project (3GPP), "Evolved Universal Terrestrial Radio Access (E-UTRA); Further advancements for E-UTRA physical layer aspects," 3rd Generation Partnership Project (3GPP), TR 36.814, Mar. 2010.

[13] ——, "Study on 3D channel model for LTE," 3rd Generation Partnership Project (3GPP), TR 36.873, Sept. 2014.

[14] H. Dhillon and J. Andrews, "Downlink rate distribution in heterogeneous cellular networks under generalized cell selection," *IEEE Wireless Communications Letters*, vol. 3, no. 1, pp. 42–45, Feb. 2014.

[15] T. Bai, R. Vaze, and R. Heath, Jr., "Analysis of blockage effects on urban cellular networks," *IEEE Transactions on Wireless Communications*, vol. 13, no. 9, pp. 5070–5083, Sept. 2014.

[16] F. Baccelli and X. Zhang, "A correlated shadowing model for urban wireless networks," in *IEEE INFOCOM'15*, Apr. 2015.

[17] F. Kakar, K. Sani, and F. Elahi, "Essential factors influencing building penetration loss," in *IEEE International Conference on Communication Technology (ICCT)*, Hangzhou, China, Nov. 2008.

[18] J.-E. Berg, "Building penetration loss at 1700 MHz along line of sight street microcells," in *IEEE International Symposium on Personal, Indoor and Mobile Radio Communications (PIMRC)*, Boston, MA, USA, Oct. 1992, pp. 86–87.

[19] R. Gahleitner and E. Bonek, "Radio wave penetration into urban buildings in small cells and microcells," in *IEEE Vehicular Technology Conference (VTC)*, Stockholm, Sweden, June 1994, pp. 887–891 vol.2.

[20] Y. Corre, J. Stephan, and Y. Lostanlen, "Indoor-to-outdoor path-loss models for femtocell predictions," in *IEEE International Symposium on Personal Indoor and Mobile Radio Communications (PIMRC)*, Toronto, ON, Canada, Sept. 2011, pp. 824–828.

[21] F. Baccelli and B. Blaszczyszyn, *Stochastic Geometry and Wireless Networks: Volume I Theory*, ser. Foundation and Trends in Networking. Delft (Netherlands): Now Publishers, March 2009.

[22] M. Taranetz, M. Rupp, R. W. Heath, Jr., and T. Bai, "Analysis of small cell partitioning in urban two-tier heterogeneous cellular networks," in *Proc. Int. Symp. on Wireless Commun. Syst. (ISWCS'14)*, Barcelona, Spain, Aug. 2014.

[23] WINNER II WP1, "WINNER II channel models," *IST-4-027756 WINNER II Deliverable D1.1.2*, Sept. 2007.

[24] J. R. Hampton, N. M. Merheb, W. L. Lain, D. E. Paunil, R. M. Shuford, and W. T. Kasch, "Urban propagation measurements for ground based communication in the military uhf band," *IEEE Tran. Antennas and Propagation*, vol. 54, no. 2, pp. 644–654, Feb 2006.

[25] B. Hanci and I. Cavdar, "Mobile radio propagation measurements and tuning the path loss model in urban areas at GSM-900 band in Istanbul-Turkey," in *IEEE Vehicular Technology Conference (VTC)*, vol. 1, Sept. 2004, pp. 139–143 Vol. 1.

[26] R. W. Heath, Jr., M. Kountouris, and T. Bai, "Modeling heterogeneous network interference using Poisson point processes," *IEEE Transactions on Signal Processing*, vol. 61, no. 16, pp. 4114–4126, Aug. 2013.

[27] T. Bai and R. W. Heath, "Coverage and rate analysis for millimeter-wave cellular networks," *IEEE Trans. Wireless Commun.*, vol. 14, no. 2, pp. 1100–1114, 2015.

[28] G. Boudreau, J. Panicker, N. Guo, R. Chang, N. Wang, and S. Vrzic, "Interference coordination and cancellation for 4G networks," *IEEE Communications Magazine*, vol. 47, no. 4, pp. 74–81, April 2009.

[29] N. Miyoshi and T. Shirai, "Downlink coverage probability in a cellular network with Ginibre deployed base stations and Nakagami-m fading channels," *CoRR*, vol. abs/1503.05377, 2015. [Online]. Available: http://arxiv.org/abs/1503.05377

[30] 3rd Generation Partnership Project (3GPP), "Evolved Universal Terrestrial Radio Access (E-UTRA) further enhancements to LTE Time Division Duplex (TDD) for Downlink-Uplink (DL-UL) interference management and traffic adaptation," 3rd Generation Partnership Project (3GPP), TR 36.828, Jun. 2012.

[31] ——, "Evolved universal terrestrial radio access (E-UTRA); radio frequency (RF) system scenarios," 3rd Generation Partnership Project (3GPP), TR 36.942, Oct. 2014.

[32] ——, "Evolved Universal Terrestrial Radio Access base station (BS) radio transmission and reception," 3rd Generation Partnership Project (3GPP), TS 36.104, Jan. 2016.

[33] H. Alzer, "On some inequalities for the incomplete Gamma function," *Mathematics of Computation*, vol. 66, no. 218, pp. 771–778, 1997. [Online]. Available: http://www.jstor.org/stable/2153894

Martin Taranetz (M'07) received the Dipl.-Ing degree (M.Sc. equivalent) (with highest distinctions) in telecommunications from the TU Wien, Wien, Austria, and the Dr.-Techn. degree (Ph.D. equivalent) (with highest Hons.) in telecommunications engineering from the TU Wien, in 2011 and 2015, respectively. In his dissertation, he focused on system level modeling and evaluation of heterogeneous cellular networks. Since 2015, he has been employed as a Project Assistant with the Mobile Communications Group, Institute of Telecommunications, TU Wien. From January 2014 to April 2014, he was a visiting researcher with the Wireless Networking and Communications Group, University of Texas at Austin, Austin, TX, USA. His research interests include wireless communications and signal processing. He was a general chair of the International Workshop on Link- and System Level Simulations (IWSLS^2). He is a reviewer for the IEEE Trans. Wireless Commun. and the IEEE Trans. Veh. Technol.

Robert W. Heath Jr. Robert W. Heath Jr. (S'96 - M'01 - SM'06 - F'11) received the B.S. and M.S. degrees from the University of Virginia, Charlottesville, VA, in 1996 and 1997 respectively, and the Ph.D. from Stanford University, Stanford, CA, in 2002, all in electrical engineering. From 1998 to 2001, he was a Senior Member of the Technical Staff then a Senior Consultant at Iospan Wireless Inc, San Jose, CA where he worked on the design and implementation of the physical and link layers of the first commercial MIMO-OFDM communication system. Since January 2002, he has been with the Department of Electrical and Computer Engineering at The University of Texas at Austin where he is a Cullen Trust for Higher Education Endowed Professor, and is a Member of the Wireless Networking and Communications Group. He is also President and CEO of MIMO Wireless Inc. and Chief Innovation Officer at Kuma Signals LLC. He is a co-author of the book Millimeter Wave Wireless Communications published by Prentice Hall in 2014.

Dr. Heath has been a co-author of several best paper award recipients including recently the 2010 and 2013 EURASIP Journal on Wireless Communications and Networking best paper awards, the 2012 Signal Processing Magazine best paper award, a 2013 Signal Processing Society best paper award, 2014 EURASIP Journal on Advances in Signal Processing best paper award, and the 2014 Journal of Communications and Networks best paper award, the 2016 IEEE Communications Society Fred W. Ellersick Prize, and the 2016 IEEE Communications and Information Theory Societies Joint Paper Award. He is an ISI Highly Cited Researcher. He is also an elected member of the Board of Governors for the IEEE Signal Processing Society, a licensed Amateur Radio Operator, and a registered Professional Engineer in Texas.

Markus Rupp Markus Rupp (F'15) received the Dipl.-Ing. degree from the University of Saarbrcken, Saarbrcken, Germany, and the Dr.-Ing. degree from the Technische Universitt Darmstadt, Darmstadt, Germany, in 1988 and 1993, respectively, where he worked with Eberhardt Hnsler. From November 1993 to July 1995, he had a Postdoctoral position with the University of Santa Barbara, Santa Barbara, CA, USA. From October 1995 to August 2001, he was a Member of Technical Staff with the Wireless Technology Research, Department of Bell-Labs, Crawford Hill, NJ, USA, where he worked on various topics related to adaptive equalization and rapid implementation for IS-136, 802.11, and UMTS. He authored and coauthored more than 500 scientific papers including 15 patents on adaptive filtering, and wireless communications. Since October 2001, he has been a Full Professor of digital signal processing in mobile communications with the Technical University of Vienna, Wien, Austria, where he served as the Dean, from 2005 to 2007 and from 2016 to 2019. He was Associate Editor of the IEEE TRANSACTIONS ON SIGNAL PROCESSING, from 2002 to 2005. He is currently a Associate Editor of EURASIP Journal of Advances in Signal Processing and EURASIP Journal on Embedded Systems. He was elected AdCom Member of EURASIP from 2004 to 2012, serving as the President of EURASIP from 2009 to 2010.